

STOCHASTIC INTERPOLANTS VIA CONDITIONAL DEPENDENT COUPLING

Chenrui Ma¹ Xi Xiao^{2,3} Tianyang Wang² Xiao Wang³ Yanning Shen^{1*}

¹University of California, Irvine, CA 92697, USA

²University of Alabama at Birmingham, Birmingham, AL 35294, USA

³Oak Ridge National Laboratory, Oak Ridge, TN 37831, USA

*Corresponding author: yannings@uci.edu

ABSTRACT

Existing image generation models face critical challenges regarding the trade-off between computation and fidelity. Specifically, models relying on a pretrained Variational Autoencoder (VAE) suffer from information loss, limited detail, and the inability to support end-to-end training. In contrast, models operating directly in the pixel space incur prohibitive computational cost. Although cascade models can mitigate computational cost, stage-wise separation prevents effective end-to-end optimization, hampers knowledge sharing, and often results in inaccurate distribution learning within each stage. To address these challenges, we introduce a unified multistage generative framework based on our proposed **Conditional Dependent Coupling** strategy. It decomposes the generative process into interpolant trajectories at multiple stages, ensuring accurate distribution learning while enabling end-to-end optimization. Importantly, the entire process is modeled as a single unified Diffusion Transformer, eliminating the need for disjoint modules and also enabling knowledge sharing. Extensive experiments demonstrate that our method achieves both high fidelity and efficiency across multiple resolutions.

1 INTRODUCTION

Generative models have achieved remarkable progress in recent years, driving advances in diverse domains such as natural language processing OpenAI et al. (2024), computer vision Geng et al. (2025a), and scientific modeling Fotiadis et al. (2024). Unlike discrete data generation (e.g., large language models for text), high-dimensional continuous data generation, such as image synthesis, suffers from high complexity and computational demands Rombach et al. (2022); Peebles & Xie (2023a); Ma et al. (2024). The primary challenge lies in balancing fidelity, efficiency, and scalability when learning to approximate intricate data distributions Sun et al. (2024); Tian et al. (2024b).

There are two main paradigms for generative modeling: pixel space generation and latent space generation. Pixel space generation operates directly in the original data domain, preserving fine-grained details without compression Bao et al. (2023); Hoogeboom et al. (2025). However, this approach suffers from extreme inefficiency due to the high dimensionality of images, resulting in expensive training and inference Rombach et al. (2022); Kingma et al. (2023). In contrast, latent space generation leverages compact representations, typically through Variational Autoencoders (VAEs), to reduce dimensionality and improve efficiency Li et al. (2024); Esser et al. (2021a). While effective, these methods inevitably incur information loss during encoding and decoding, and often cannot be trained in a fully end-to-end manner with the generative backbone Jin et al. (2024); Jiao et al. (2025).

To mitigate these limitations, multi-stage generation methods have been proposed. By decomposing the synthesis process into a sequence of stages, they allow early stages to operate in lower-dimensional spaces and later stages to refine the outputs at higher resolutions Tian et al. (2024b); Chen et al. (2025). This hierarchical design improves efficiency and progressively captures data complexity Li et al. (2025); Ren et al. (2024). Nonetheless, existing multi-stage frameworks rely on disentangled stage-specific models, preventing unified parameterization and end-to-end optimiza-

tion Ho et al. (2022b); Kim et al. (2024). Furthermore, the decoupled design may lead to inaccurate distribution modeling, with errors compounding across stages Chen et al. (2025); Jin et al. (2024).

In this work, we propose a novel multi-stage generation framework based on *stochastic interpolant* Albergo et al. (2023a); Albergo & Vanden-Eijnden (2022) with **conditional dependent coupling**. Our approach generates high-resolution images in a coarse-to-fine manner, essentially addressing the notorious limitations of the multi-stage generation paradigm. Specifically, the proposed method enables efficient and high-performance generation directly in pixel space, thus retaining detailed information without the bottleneck of latent compression. Moreover, by proposing **conditional dependent coupling**, we unify the multi-stage generation process into one coherent framework, ensuring accurate distribution learning at each stage. Notably, the entire multi-stage framework can be parameterized by a single DiT Peebles & Xie (2023b), facilitating knowledge sharing across stages and enabling full end-to-end optimization. We further provide formal proof that the proposed framework significantly reduces the transport cost and inference time. See the Related Works in the Appendix. The source code will be made publicly available upon acceptance.

2 PRELIMINARIES

The *stochastic interpolant* Albergo et al. (2023a); Albergo & Vanden-Eijnden (2022) unifies the theory of Ordinary Differential Equations (ODEs) and Stochastic Differential Equations (SDEs). Our method, which was developed based on this theory, is therefore comparable to both the Flow/ODEs and Diffusion/SDEs generation. For notation simplicity and efficient information delivery, in the rest of the paper, we focus on the Flow/ODEs. However, the complete *stochastic interpolant* theory that introduces an additional noise term and recovers Diffusions/SDEs is presented in Appendix §C, where we show that the deterministic interpolant definitions below can be generalized readily.

Definition 1 (Deterministic interpolant for Flow Matching). Given two probability densities $\rho_0, \rho_1 : \mathbb{R}^d \rightarrow \mathbb{R}_{\geq 0}$ and a coupling $\rho(x_0, x_1)$ with marginals ρ_0 and ρ_1 , we define the deterministic interpolant Lipman et al. (2024; 2022):

$$I_t = \alpha_t x_0 + \beta_t x_1, \quad t \in [0, 1], \quad (1)$$

where α_t, β_t are differentiable in t and satisfy the boundary conditions:

$$\alpha_0 = \beta_1 = 1, \quad \alpha_1 = \beta_0 = 0, \quad \alpha_t^2 + \beta_t^2 > 0 \quad \forall t \in [0, 1].$$

This yields a time-dependent density ρ_t for I_t with $\rho_{t=0} = \rho_0$ and $\rho_{t=1} = \rho_1$.

Theorem 1 (Transport continuity equation for Flow model). *Let $b_t : \mathbb{R}^d \rightarrow \mathbb{R}^d$ denote the conditional velocity field Lipman et al. (2024; 2022):*

$$b_t(x) = \mathbb{E} \left[\dot{I}_t \mid I_t = x \right], \quad (2)$$

where $\dot{f} = \frac{df}{dt}$ and the expectation is over $(x_0, x_1) \sim \rho(x_0, x_1)$. The interpolant density ρ_t solves the transport continuity equation Villani et al. (2008); Villani (2021):

$$\partial_t \rho_t(x) + \nabla \cdot (b_t(x) \rho_t(x)) = 0. \quad (3)$$

In practice, we learn a model velocity b_t to approximate b_t by minimizing:

$$L_b(\hat{b}) = \int_0^1 \mathbb{E} \left[|\hat{b}_t(I_t)|^2 - 2 \dot{I}_t \cdot \hat{b}_t(I_t) \right] dt, \quad (4)$$

which is estimable from samples $(x_0, x_1) \sim \rho(x_0, x_1)$.

Corollary 1 (Probability flow ODE). *The transport continuity equation implies that the solution X_t to the probability flow ODE Song et al. (2023); Ma et al. (2024):*

$$\dot{X}_t = b_t(X_t) \quad (5)$$

matches the interpolant law: if $X_{t=0} \sim \rho_0$, then $X_{t=1} \sim \rho_1$. Hence generative sampling is obtained by drawing $x_0 \sim \rho_0$ and integrating equation 5 from $t=0$ to $t=1$.

Remark (Generalization to stochastic interpolant). The Appendix §C introduces the full *stochastic interpolant* $I_t = \alpha_t x_0 + \beta_t x_1 + \gamma_t z$ with $z \sim \mathcal{N}(0, I_d)$, Albergo et al. (2023a); Albergo & Vanden-Eijnden (2022) which recovers diffusion-type models, the score field $s_t(x) = \nabla \log \rho_t(x)$,

and the companion objective for s_t . All transport-equation statements above remain valid, with equation 2–equation 5 appearing as the $\gamma_t \equiv 0$ case used throughout the main text.

Definition 2 (Transport cost). Let $X_t(x_0)$ be the solution to the probability flow ODE equation 5 for the initial condition $X_{t=0}(x_0) = x_0 \sim \rho_0$. Then the following inequality holds:

$$\mathbb{E}_{x_0 \sim \rho_0} [|X_{t=1}(x_0) - x_0|^2] \leq \int_0^1 \mathbb{E}[|\dot{I}_t|^2] dt < \infty. \quad (6)$$

Minimizing the left-hand side of equation 6 would achieve the optimal transport in the sense of Benamou-Brenier Benamou & Brenier (2000), and the minimum would give the Wasserstein-2 distance between ρ_0 and ρ_1 Albergo et al. (2023b).

While for a common *stochastic interpolant*, this transport cost construction was made using the choice $\rho(x_0, x_1) = \rho_0(x_0)\rho_1(x_1)$, so that x_0 and x_1 were drawn independently from the base and the target, **data-dependent coupling** constructs the joint distribution by $\rho(x_0, x_1) = \rho_0(x_0 | x_1)\rho_1(x_1)$ to reduce the transport cost Albergo et al. (2023b), such that:

$$\int_{\mathbb{R}^{3d}} |\dot{I}_t|^2 \rho(x_0, x_1) \rho_z(z) dx_0 dx_1 dz \leq \int_{\mathbb{R}^{3d}} |\dot{I}_t|^2 \rho_0(x_0) \rho_1(x_1) \rho_z(z) dx_0 dx_1 dz, \quad (7)$$

The bound on the transportation cost in equation 6 is more tightly controlled by the construction of data-dependent couplings Albergo et al. (2023b).

3 METHODOLOGY

In this section, we introduce a unified multi-stage generative algorithm designed to efficiently produce high-resolution images without relying on a pretrained VAE, thereby mitigating information and detail loss while enabling end-to-end training. The algorithm proceeds through a sequence of stages, where the resolution is progressively refined in a coarse-to-fine manner. At each stage, the output of the previous stage is further enhanced toward a finer resolution target using *stochastic interpolant* with **conditionally dependent coupling**, thus forming a cascaded architecture and guaranteeing accurate data distribution modeling at each stage. Crucially, all stages are parameterized by a single unified DiT Peebles & Xie (2023a), which facilitates knowledge sharing and supports end-to-end optimization. Under the *stochastic interpolant* framework, the proposed method is naturally compatible with Flow models (ODEs) as well as Diffusion models (SDEs). For clarity, we focus here on deterministic interpolants (Flow/ODEs), while noting that the method extends readily to stochastic interpolants (includes Diffusion/SDEs), see Preliminary for details.

3.1 NOTATIONS

Data and Resolution Hierarchy. Let the target high-resolution image distribution be defined on \mathbb{R}^{d_K} . We define a hierarchy of resolutions, where $k \in \{1, \dots, K\}$ represents the generation stage: **1** $x^{(K)} \sim p_{\text{data}}$: A sample from the true high-resolution data distribution. **2** $x_1^{(k)} \in \mathbb{R}^{d_k}$: A ground-truth image sample at stage k , which is generated by downsampling the original high-resolution image.

Upsampling and Downsampling Operators. We define operators for changing image resolutions. Let the scaling factor between stage $k-1$ and k be a power of 2: $d_k = 2^{k-1}d_1$, for simplicity.

- **Downsampling Operator D_k** : This operator maps an image from resolution d_k to d_{k-1} ($D_k : \mathbb{R}^{d_k} \rightarrow \mathbb{R}^{d_{k-1}}$). It operates via neighborhood averaging, where a block of pixels in the higher-resolution image is averaged to a single pixel in the lower-resolution image.
- **Upsampling Operator U_k** : This operator maps an image from resolution d_{k-1} to d_k ($U_k : \mathbb{R}^{d_{k-1}} \rightarrow \mathbb{R}^{d_k}$). It operates via neighborhood replication, where each pixel from the lower-resolution image is copied to form a block in the higher-resolution image.

These operators are defined such that they are transitive: $D_{k+1 \rightarrow k-1} = D_k \circ D_{k+1}$. We can define a composite downsampling operator $D_{K \rightarrow k}$ that maps from the highest resolution d_K directly to d_k . The ground-truth sample for any stage k is thus defined as $x_1^{(k)} = D_{K \rightarrow k}(x^{(K)}) \sim \rho_1^{(k)}(x_1^{(k)} | x^{(K)})$.

3.2 MULTI-STAGE FLOW MATCHING MODEL

To implement the unified multi-stage generation process, we define a single unified generative model (Flow/ODEs or Diffusion/SDEs) to transform from the source distribution to the target at each stage k with **conditional dependent coupling**. The K stages are designed as below: **1 Stage $k = 1$: Noise-to-Image Generation.** The first stage generates a low-resolution image from a simple source distribution (e.g., Gaussian noise). **2 Stage $k > 1$: Image-to-Image Refinement.** In subsequent stages, the resolution is progressively refined by leveraging **conditionally dependent coupling**, where the probability path is explicitly conditioned on the relationship between the low-resolution source and the high-resolution target images. This cascaded approach breaks down the complex task of high-resolution image generation into a series of more manageable sub-problems. We will elaborate on the **motivation** and **benefits** of the design at the end of this section.

Stage $k = 1$: Noise-to-Image Generation The first stage ($k = 1$) of our model is responsible for generating the lowest-resolution image from a simple prior distribution. The model is defined by its source and target distributions and the **conditional dependent coupling** between them. For this foundational stage, the joint distribution is the product of the marginals:

$$\begin{aligned} \rho^{(1)}(x_0^{(1)}, x_1^{(1)} | x^{(K)}) &= \rho_0^{(1)}(x_0^{(1)} | x_1^{(1)}) \rho_1^{(1)}(x_1^{(1)} | x^{(K)}) \\ &= \rho_0^{(1)}(x_0^{(1)}) \rho_1^{(1)}(x_1^{(1)} | x^{(K)}) \end{aligned} \quad (8)$$

The **target distribution** is the empirical distribution of the lowest-resolution ground-truth images, where $x_1^{(1)} \sim \rho_1^{(1)}(x_1^{(1)} | x^{(K)})$. The **source distribution** is a standard Gaussian distribution denoted as $x_0^{(1)} \sim \rho_0^{(1)}(x_0^{(1)}) = \mathcal{N}(0, \sigma^2 I_{d_1})$, which is independent to $\rho_1^{(1)}(x_1^{(1)} | x^{(K)})$, where can also drive that $\rho_0^{(1)}(x_0^{(1)} | x_1^{(1)}) = \rho_0^{(1)}(x_0^{(1)})$ from equation 8.

Stage $k > 1$: Image-to-Image Refinement For all subsequent stages ($k > 1$), the model learns to perform a coarse-to-fine resolution enhancement. The core of these stages is the **conditional dependent coupling** that leverages the structural similarity between the lower-resolution source image and the higher-resolution target image. For each stage k , the **target distribution** is the distribution of ground-truth images $x_1^{(k)} \sim \rho_1^{(k)}(x_1^{(k)} | x^{(K)})$ at resolution d_k . Instead of drawing from a simple prior, the **source sample** $x_0^{(k)}$ is constructed directly from the corresponding target sample $x_1^{(k)}$: $x_0^{(k)} \sim \rho_0^{(k)}(x_0^{(k)} | x_1^{(k)})$. This is achieved by first applying a deterministic mapping $m_k(x_1^{(k)}) = U_k(D_k(x_1^{(k)}))$ and then adding a small amount of Gaussian noise to ensure the conditional probability is well-defined:

$$x_0^{(k)} = m_k(x_1^{(k)}) + \sigma_k \zeta_k = U_k(D_k(x_1^{(k)})) + \sigma_k \zeta_k \quad (9)$$

where $\zeta_k \sim \mathcal{N}(0, I_{d_k})$ and σ_k is a small, stage-dependent noise level, which can be tuned. This construction induces a conditional probability $\rho_0^{(k)}(x_0^{(k)} | x_1^{(k)})$ and a joint probability density $\rho^{(k)}(x_0^{(k)}, x_1^{(k)} | x^{(K)})$:

$$\rho_0^{(k)}(x_0^{(k)} | x_1^{(k)}) = \mathcal{N}(x_0^{(k)}; m_k(x_1^{(k)}), \sigma_k^2 I_{d_k}) \quad (10)$$

$$\rho^{(k)}(x_0^{(k)}, x_1^{(k)} | x^{(K)}) = \rho_0^{(k)}(x_0^{(k)} | x_1^{(k)}) \rho_1^{(k)}(x_1^{(k)} | x^{(K)}) \quad (11)$$

Model Parameterization We design a unified DiT model that operates consistently across multiple resolutions by sharing a single set of parameters. To enable the model to recognize and differentiate between these resolutions, we introduce an additional resolution embedding. Specifically, we treat the absolute resolution of the feature map r_k obtained after patch embedding Dosovitskiy et al. (2020) as a conditional signal. This signal is then encoded using sinusoidal positional embeddings Vaswani et al. (2017) $e_k = E(r_k)$ and fused with the timestep embedding by the cross-attention mechanism Vaswani et al. (2017) before being fed into the model.

To unify the multi-stage generation, the rescaled timestep strategy Chen et al. (2025); Jin et al. (2024); Yan et al. (2024) is employed to align the multi-stage generation time definition with the standard Flow model Lipman et al. (2022), which generates across the time scope $t \in [0, 1]$. For each stage k , the start time point and end time point are defined as t_0^k and t_1^k , where $0 \leq t_0^k < t_1^k \leq 1$,

$t_0^k = t_1^{k-1}$, and meet boundary condition $t_0^1 = 0$, $t_1^K = 1$. For simplicity, we construct a linear interpolant by specifying $\alpha_t = 1 - \tau$ and $\beta_t = \tau$ in Definition 1:

$$I_\tau^{(k)} = (1 - \tau) \cdot x_0^{(k)} + \tau \cdot x_1^{(k)}, \quad (12)$$

where $\tau = \frac{t - t_0^k}{t_1^k - t_0^k}$, so that timestep $t \in [0, 1]$ of the entire multi-stage generation process located in each stage k : $t \in [t_0^k, t_1^k]$ is rescaled to $\tau \in [0, 1]$ within each stage k .

The single unified DiT is parameterized by b^θ to model all generation stages. For the deterministic interpolant (Flow/ODEs), derived from equation 4, the DiT is optimized by:

$$\mathcal{L}(\theta) = \mathbb{E}_{t \sim [0, 1], k, e_k, (x_0^{(k)}, x_1^{(k)}) \sim \rho^{(k)}(x_0^{(k)}, x_1^{(k)} | x^{(K)})} \left[\left| b^\theta(I_\tau^{(k)}, \tau, e_k) \right|^2 - 2\dot{I}_\tau^{(k)} \cdot b^\theta(I_\tau^{(k)}, \tau, e_k) \right] \quad (13)$$

where $k = \arg_k \{ t \in [t_0^k, t_1^k] \}$, and $\dot{I}_\tau^{(k)} = x_1^{(k)} - x_0^{(k)}$.

3.3 CONDITIONAL DEPENDENT COUPLING

For the multi-stage generation model proposed in Sec. 3.2, we employed the **conditional dependent coupling** strategy to unify them. Instead of mapping unstructured noise to an image, our approach maps a structured prior—the upsampled low-resolution image from the previous stage with added stage-dependent noise—to the target high-resolution distribution. The joint probability distribution of the entire multi-stage interpolant with **conditional dependent coupling** is expressed as:

$$\begin{aligned} \rho(x_1^{(K)}, x_0^{(K)}, x_1^{(K-1)}, \dots, x_0^{(2)}, x_1^{(1)}, x_0^{(1)}) &= \rho(x^{(K)}) \prod_{k=1}^K \rho^{(k)}(x_0^{(k)}, x_1^{(k)} | x^{(K)}) \\ &= \rho(x^{(K)}) \prod_{k=1}^K \rho_0^{(k)}(x_0^{(k)} | x_1^{(k)}) \rho_1^{(k)}(x_1^{(k)} | x^{(K)}), \end{aligned} \quad (14)$$

This formulation reveals a key property of our model. Conditioned on the final high-resolution image $x^{(K)}$, the data coupling at any given stage k , denoted as $\rho^{(k)}(x_0^{(k)}, x_1^{(k)} | x^{(K)})$, is independent of that at any other stage $k^* \neq k$:

$$\rho^{(k)}(x_0^{(k)}, x_1^{(k)} | x^{(K)}) \perp\!\!\!\perp \rho^{(k^*)}(x_0^{(k^*)}, x_1^{(k^*)} | x^{(K)}), \quad (15)$$

Sequential dependency as Markov chain This conditional independence establishes a foundational **Markov chain** Norris (1998) structure across the stages. Consequently, the generative process at inference time proceeds sequentially as follows:

$$\begin{aligned} \rho(\hat{x}_0^{(1)}, \hat{x}_1^{(1)}, \hat{x}_0^{(2)}, \dots, \hat{x}_1^{(K-1)}, \hat{x}_0^{(K)}, \hat{x}_1^{(K)}) &= \rho^{(1)}(\hat{x}_0^{(1)}, \hat{x}_1^{(1)}) \prod_{k=2}^K \rho^{(k)}(\hat{x}_0^{(k)}, \hat{x}_1^{(k)} | \hat{x}_1^{(k-1)}) \\ &= \rho_0^{(1)}(\hat{x}_0^{(1)}) \rho_1^{(1)}(\hat{x}_1^{(1)} | \hat{x}_0^{(1)}) \prod_{k=2}^K \rho_1^{(k)}(\hat{x}_1^{(k)} | \hat{x}_0^{(k)}) \rho_0^{(k)}(\hat{x}_0^{(k)} | \hat{x}_1^{(k-1)}), \end{aligned} \quad (16)$$

Here, the initial prior $\rho_0^{(1)}(\hat{x}_0^{(1)})$ is a standard normal distribution, $\mathcal{N}(\hat{x}_0^{(1)}; 0, I_{d_1})$. The conditional distributions $\rho_1^{(k)}(\hat{x}_1^{(k)} | \hat{x}_0^{(k)})$ for all stages k are parameterized by a single unified generative model b^θ . For the refinement stages ($k \geq 2$), the conditional prior $\rho_0^{(k)}(\hat{x}_0^{(k)} | \hat{x}_1^{(k-1)})$ is defined by the deterministic upsampling step with added Gaussian noise:

$$\rho_0^{(k)}(\hat{x}_0^{(k)} | \hat{x}_1^{(k-1)}) = \mathcal{N}(\hat{x}_0^{(k)}; U_k(\hat{x}_1^{(k-1)}), \sigma_k^2 I_{d_k}), \quad (17)$$

which is implemented by sampling $\hat{x}_0^{(k)} = U_k(\hat{x}_1^{(k-1)}) + \sigma_k \zeta_k$, akin with the distribution formed by equation 9. In contrast to previous autoregressive modeling methods that severely limited by the computational complexity arising from the full-resolution long-history condition Tian et al. (2024b); Ren et al. (2025), and potential complex token/feature pyramid construction Jiao et al. (2025), the proposed generative process begins with a sample from the simple prior: $\hat{x}_0^{(1)} \sim \rho_0^{(1)}(\hat{x}_0^{(1)})$, sub-

sequently, the output of each stage $\hat{x}_1^{(k-1)}$ serves as the basis for the input to the next stage $\hat{x}_0^{(k)}$, forming the sequential dependency characteristic of a Markov chain, as shown in equation 16.

Reducing transport cost **Conditional dependent coupling** strategy integrating each stage and thus decreasing transport cost $L = \int_0^1 \mathbb{E}[|\dot{I}_t|^2]dt < \infty$ as defined in Definition 2, see in Theorem 2.

Theorem 2. *The transport cost of the naive single-stage model, which generates a high-resolution image $\hat{x}_1 \sim x^{(K)} \in \mathbb{R}^{d_K}$ directly from Gaussian noise $x_0 \sim \mathcal{N}(0, \sigma^2 I_{d_K})$ (denoted as L_A), is greater than that of the proposed multi-stage model with conditional dependent coupling strategy, which generates a high-resolution image $\hat{x}_1^{(K)} \sim x^{(K)} \in \mathbb{R}^{d_K}$ from Gaussian noise $x_0^{(1)} \sim \mathcal{N}(0, \sigma^2 I_{d_1})$ through K stages (denoted as L_B). Specifically, we have $L_A > L_B$.*

$$L_A = \mathbb{E}[|x_1|^2] + \mathbb{E}[|x_0|^2] > L_B = \sum_{k=1}^K L_k, \quad (18)$$

where L_k denotes the transport cost at the k -th stage. See proof in Appendix §D.1.

Accurate distribution learning In contrast to existing unified multi-stage generation methods Chen et al. (2025); Jin et al. (2024), the proposed method guarantees that the model b^θ learns the accurate data distribution $\rho_1^{(k)}(x_1^{(k)} | x^{(K)})$ at each stage. This, in turn, enables the unified generative model to capture the target high-resolution image distribution $x^{(K)} \sim p_{\text{data}}$ by progressively matching $\rho_1^{(k)}(x_1^{(k)} | x^{(K)})$ at every stage k . As an example, consider conditional generation: $b^\theta(I_\tau^{(k)}, \tau, e_k)$ models stage- k generation by solving the ODE $\dot{X}_\tau^k = b^\theta(I_\tau^{(k)}, \tau, e_k)$, where $b^\theta(I_\tau^{(k)}, \tau, e_k) = \mathbb{E}_{\mathbf{c}}[b^\theta(I_\tau^{(k)}, \tau, e_k, \mathbf{c})]$ and \mathbf{c} denotes the conditioning signal (e.g., class label, text prompt). Conditional generation toward conditions \mathbf{c}_1 and \mathbf{c}_2 within stage k is given by

$$I_{1,\mathbf{c}_1}^{(k)} = I_\tau^{(k)} + \int_\tau^1 b^\theta(I_t^{(k)}, t, e_k, \mathbf{c}_1)dt, \quad I_{1,\mathbf{c}_2}^{(k)} = I_\tau^{(k)} + \int_\tau^1 b^\theta(I_t^{(k)}, t, e_k, \mathbf{c}_2)dt, \quad (19)$$

where $I_\tau^{(k)}$ denotes the current sample at the rescaled timestep $\tau \in [0, 1]$ within stage k , and specifically $I_0^{(k)}$ denotes the starting point of stage k .

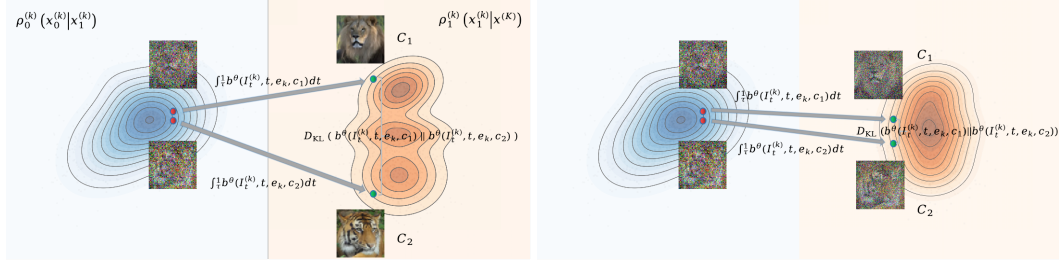


Figure 1: Data Distribution Learning and Transition.

In the initial and intermediate stages, $I_\tau^{(k)}$ approximately follows a standard Gaussian—structureless and semantically vague—due to low resolution and high noise levels, and is therefore not characterizable. Consequently, we assume that the current sample $I_\tau^{(k)}$ used to generate $I_{1,\mathbf{c}_1}^{(k)}$ and $I_{1,\mathbf{c}_2}^{(k)}$ is identical within an initial or intermediate stage k ; see the red point in Figure 1.

For previous multi-stage methods Chen et al. (2025); Jin et al. (2024) that maintain noise in the target across stage $k < K$, the initial and intermediate stages necessarily target structureless, semantically vague data (close to standard Gaussian noise) due to low resolution and high noise levels. As a result, the model b^θ cannot learn accurate condition-specific distributions for \mathbf{c}_1 and \mathbf{c}_2 , as indicated by a small divergence $D_{\text{KL}}(b^\theta(I_t^{(k)}, t, e_k, \mathbf{c}_1) || b^\theta(I_t^{(k)}, t, e_k, \mathbf{c}_2))$; see the right part of Figure 1.

However, under the proposed training strategy with **conditional dependent coupling**, which treats the accurate data distribution $\rho_1^{(k)}(x_1^{(k)} | x^{(K)}) = \mathbb{E}_{\mathbf{c}}[\rho_1^{(k)}(x_1^{(k)} | x^{(K)}, \mathbf{c})]$ as the target at each stage—where $\rho_1^{(k)}(x_1^{(k)} | x^{(K)}, \mathbf{c})$ denotes the condition-specific distribution of condition \mathbf{c} —the

multi-stage generator b^θ is guaranteed to learn the information and details pertinent to stage k by transforming the source distribution $\rho_0^{(k)}(x_0^{(k)} \mid x_1^{(k)})$ into the accurate target distribution $\rho_1^{(k)}(x_1^{(k)} \mid x^{(K)})$ at stage k for every condition \mathbf{c} . This is reflected by an adequate divergence $D_{\text{KL}}\left(b^\theta(I_t^{(k)}, t, e_k, \mathbf{c}_1) \parallel b^\theta(I_t^{(k)}, t, e_k, \mathbf{c}_2)\right)$; see the left part of Figure 1.

3.4 CLASSIFIER-FREE GUIDANCE FOR CONDITIONAL DEPENDENT COUPLING

Thanks to the accurate data distribution modeling at each stage k , Classifier-Free Guidance (CFG) Ho & Salimans (2022) can be seamlessly integrated with **conditional dependent coupling**. This eliminates the need for a stage-wise CFG schedule Chen et al. (2025); Kynkänniemi et al. (2024), which otherwise requires carefully assigning the CFG strength at every stage, thereby ensuring both elegance and ease of implementation. In the proposed method, a single CFG strength S_{cfg} is applied uniformly across all stages k . Further details are provided in Appendix §F.

3.5 ALGORITHM WORKFLOWS

Here we present the detailed unconditional training and inference procedures for the unified multi-stage generative model b^θ with **conditional dependent coupling** in Appendix §E. The inference steps are described using the forward Euler method Lipman et al. (2024; 2022) for solving the ODE, as a simple example of a numerical solver. Moreover, the detailed training and inference procedures for modeling b^θ in conditional generation with CFG are provided in Appendix §F.

4 THEORETICAL JUSTIFICATION AND KEY PROPERTY

Mathematical premise and intuition. Our method adopts a unified multi-scale, coarse-to-fine image generation procedure that aligns with the natural way humans recognize images. Compared to previous coarse-to-fine AR approaches Tian et al. (2024a); Ren et al. (2025), our method is based on a unified and continuous transformation between distributions in a highly controllable manner, which better reflects the smooth nature of image transitions. Compared to existing multi-stage generation methods Ho et al. (2022a), our method models a unified multi-stage generation process with **conditional dependent coupling** and can be parameterized by a single DiT that can be trained from end-to-end. Furthermore, due to the accurate distribution modeling at each stage, our method is guaranteed to learn the target high-quality data distribution by progressively matching the data distribution at each stage. This resolves the generation problem step by step within a unified process.

Diversity and stochasticity. In image generation, diversity—typically introduced by the stochasticity of generative models—is primarily expressed in the early stages (initial transition steps for ODE/SDE) Chen et al. (2025); Tian et al. (2024b). For the proposed method, this corresponds to the transition modeled in the initial and intermediate stages. During these stages, key attributes like object presence, layout, and structure are determined. In contrast, the subsequent high-resolution refinement stages require less diversity. By employing the proposed **conditional dependent coupling** strategy, we explicitly decouple the diverse coarse image generation from the fine image refinement, thereby achieving both high performance and efficiency. Specifically, as the stage index k increases, we gradually reduce the stage-dependent noise level σ_k in equation 9. This adjustment improves both training and inference efficiency while maintaining strong performance, defined as

$$\sigma_k = \gamma^{-(k-1)} \sigma, \quad \text{where } \gamma \geq 1, \quad 2 \leq k \leq K. \quad (20)$$

We refer to γ as the "diminish factor" and further analyze its impact in our experiments.

Few-step generation and Efficient inference. Although not originally designed as such, the generative task modeled by the proposed unified multi-stage method with **conditional dependent coupling** is decomposed into subtasks within each generation stage. This decomposition regularizes the overall generation trajectory into multiple straighter sub-trajectories, thereby reducing the number of function evaluations (NFE) required at each stage Frans et al. (2024); Geng et al. (2025b). Moreover, the simulations in the early stages are substantially faster than those in the final stage, which targets the full-resolution image. Quantitatively, this approach leads to a significant reduction in the transport cost, as established in Theorem 2. Consequently, fewer steps are needed to obtain qualified results, and the overall inference time is shortened. Here we summarize as Theorem 3 below.

Theorem 3. The inference time of the naive single-stage model, which generates a high-resolution image $\hat{x}_1 \sim x^{(K)} \in \mathbb{R}^{d_K}$ directly from Gaussian noise $x_0 \sim \mathcal{N}(0, \sigma^2 I_{d_K})$ (denoted as T_A), is greater than that of the proposed multi-stage model with a conditional dependent coupling strategy, which generates a high-resolution image $\hat{x}_1^{(K)} \sim x^{(K)} \in \mathbb{R}^{d_K}$ from Gaussian noise $x_0^{(1)} \sim \mathcal{N}(0, \sigma^2 I_{d_1})$ through K stages (denoted as T_B). Specifically, we have $T_A > T_B$.

$$T_A = \mathbb{E}[\iota(x_0 \rightarrow \hat{x}_1)] > T_B = \sum_{k=1}^K \mathbb{E}[\iota(x_0^{(k)} \rightarrow \hat{x}_1^{(k)})], \quad (21)$$

where $\iota(\cdot)$ denotes the expected inference time cost of generating the target image from the input sample at each stage. See proof in Appendix §D.2.

5 EXPERIMENT

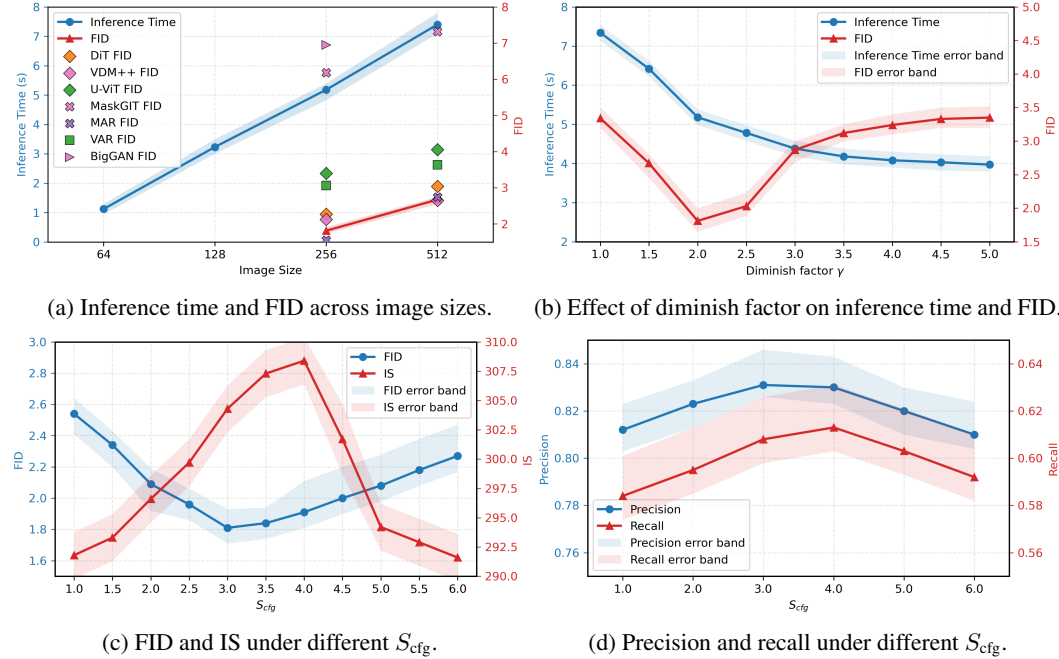
To comprehensively evaluate the effectiveness of the proposed unified multi-stage generation model with **conditional dependent coupling** (CDC-FM), we conduct extensive experiments.

Class-conditional image generation. In Table 1, we compare CDC-FM with various existing methods, including GANs, Autoregressive(AR) models, Diffusion/Flow Matching models, and Multi-stage models in the ImageNet-1k/256 benchmark Krizhevsky et al. (2012), which represent current state-of-the-art generative performance.

Furthermore, we also report the comparison result of the ImageNet-1k/512 benchmark Krizhevsky et al. (2012) in Table 2, which shows the robustness of our method in higher resolution.

We visualize the class-conditional image generation result of our method in Figure 3, demonstrating high-fidelity, accuracy, and diversity across all the classes.

Inference Efficiency. Thanks to the disentangled design of each generation stage in the proposed multi-stage generation model with **conditional dependent coupling**, we explicitly separate coarse image generation from fine image refinement. This disentanglement enables both efficient inference and training while maintaining strong performance. Table 1 reports a comparison of inference time costs between representative methods with CDC-FM under varying numbers of function evaluations (NFE) on the ImageNet-1k/256 benchmark. Furthermore, we measure the inference time of CDC-FM at varying image resolutions: $\{64, 128, 256, 512\}$ on the ImageNet-1k benchmark. Figure 2a showcases the trend that the inference time of the proposed multi-stage generative model with **conditional dependent coupling** is linear to the generated image size, which coincides with Theorem 3



	Model/Method	Params	FID ↓	IS ↑	Precision ↑	Recall ↑	NFE	Speed
GAN	BigGAN Brock et al. (2019)	112M	6.95	224.5	0.89	0.38	1	1.46
	GigaGAN Kang et al. (2023)	569M	3.45	225.5	0.84	0.61	1	1.32
	StyleGAN Karras et al. (2019)	166M	2.30	265.1	0.78	0.53	1	0.96
Diffusion / Flow	ADM Dhariwal & Nichol (2021)	554M	10.94	101.0	0.69	0.63	250×2	9.46
	U-ViT Bao et al. (2023)	287M	3.40	219.9	0.83	0.52	-	-
	LDM-4-G Rombach et al. (2022)	400M	3.60	247.7	-	-	250×2	4.18
	DiT-XL/2 Peebles & Xie (2023a)	675M	2.27	278.2	0.83	0.57	250×2	3.66
	SiT-XL/2 Ma et al. (2024)	675M	2.06	270.3	0.82	0.59	250×2	3.53
	VDM++ Kingma et al. (2023)	2.0B	2.12	267.7	-	-	-	-
	SiD Hoogeboom et al. (2023)	2.0B	2.77	211.8	-	-	512×2	10.12
token-wise AR	SiD2 Hoogeboom et al. (2025)	2.0B	1.72	-	-	-	-	-
	JetFormer Tschannen et al. (2024)	2.8B	6.64	-	0.69	0.56	-	-
	VQVAE-2 Razavi et al. (2019)	13.5B	31.11	45.0	0.36	0.57	-	-
	ViT-VQGAN Yu et al. (2021)	1.7B	4.17	175.1	-	-	-	-
	VQGAN Esser et al. (2021b)	1.4B	15.78	74.3	-	-	1024	12.76
	RQTransformer Lee et al. (2022)	3.8B	7.55	134.0	-	-	-	-
	LlamaGen-B Sun et al. (2024)	111M	5.46	193.6	0.83	0.45	-	-
Masked AR	LlamaGen-L Sun et al. (2024)	343M	3.07	256.1	0.83	0.52	-	-
	LlamaGen-XL Sun et al. (2024)	775M	2.62	244.1	0.80	0.57	-	-
	LlamaGen-3B Sun et al. (2024)	3.1B	2.18	263.3	0.81	0.58	-	-
	MaskGIT Chang et al. (2022)	227M	6.18	182.1	0.80	0.51	8	0.97
scale-wise AR	RCG Li et al. (2023)	502M	3.49	215.5	-	-	-	-
	MAR-B Li et al. (2024)	208M	2.31	281.7	0.82	0.57	-	-
	MAR-L Li et al. (2024)	479M	1.78	296.0	0.81	0.60	-	-
	MAR-H Li et al. (2024)	943M	1.55	303.7	0.81	0.62	256×2	1.23
	FlowAR-S Ren et al. (2024)	170M	3.61	234.1	0.83	0.50	-	-
	FlowAR-B Ren et al. (2024)	300M	2.90	272.5	0.84	0.54	-	-
	FlowAR-L Ren et al. (2024)	589M	1.90	281.4	0.83	0.57	-	-
Multi-stage	FlowAR-H Ren et al. (2024)	1.9B	1.65	296.5	0.83	0.60	-	-
	VAR-d16 Tian et al. (2024b)	310M	3.30	274.4	0.84	0.51	-	-
	VAR-d20 Tian et al. (2024b)	600M	2.57	302.6	0.83	0.56	-	-
	VAR-d24 Tian et al. (2024b)	1.0B	2.09	312.9	0.82	0.59	-	-
	VAR-d30 Tian et al. (2024b)	2.0B	1.92	323.1	0.82	0.59	10×2	1.12
	CDM Ho et al. (2022b)	-	4.88	158.7	-	-	-	-
	PixelFlow Chen et al. (2025)	677M	1.98	282.1	0.81	0.60	-	-
CDC-FM (ours)	RIN Jabri et al. (2022)	410M	3.42	182.0	-	-	-	-
	PaGoDA Kim et al. (2024)	0.9B	1.56	259.6	-	0.59	-	-
	FractalMAR-B Li et al. (2025)	186M	11.80	274.3	0.78	0.29	-	-
	FractalMAR-L Li et al. (2025)	438M	7.30	334.9	0.79	0.44	-	-
	FractalMAR-H Li et al. (2025)	848M	6.15	348.9	0.81	0.46	-	-
	CDC-FM (ours)	677M	1.97	298.2	0.80	0.58	$2 \times 4 \times 2$	1.31
	CDC-FM (ours)	677M	1.87	301.8	0.82	0.60	$4 \times 4 \times 2$	2.66
CDC-FM (ours)	CDC-FM (ours)	677M	1.81	304.3	0.83	0.61	$6 \times 4 \times 2$	5.18

Table 1: Comprehensive comparison of generative models on ImageNet-1k/256. Missing values are denoted “-”. In the NFE field, “ $\times 2$ ” indicates that CFG incurs an NFE of 2 per sampling step.

Table 2: Comparison on ImageNet-1k/512 conditional generation. Missing values are denoted “-”.

Model/Method	Params	FID ↓	IS ↑
BigGAN	-	8.43	177.9
ADM Dhariwal & Nichol (2021)	554M	7.72	172.7
VDM++ Kingma et al. (2023)	2B	2.65	278.1
DiT-XL/2 Peebles & Xie (2023a)	675M	3.04	240.8
U-ViT Bao et al. (2023)	501M	4.05	263.8
SiD2 Hoogeboom et al. (2025)	2.0B	2.19	-
MaskGIT Chang et al. (2022)	227M	7.32	156.0
MAGGIT-v2 Yu et al. (2025)	307M	3.07	324.3
MAR-L Li et al. (2024)	481M	2.74	205.2
VQGAN Esser et al. (2021b)	1.4B	26.52	66.8
VAR-d36-s Tian et al. (2024b)	2.0B	2.63	303.2
PaGoDA Kim et al. (2024)	0.9B	1.80	251.3
CDC-FM	684M	2.65	307.4

Classifier-free Guidance. As discussed in Sec. 3.4, we employ a constant CFG strength S_{cfg} across all stages. This strategy is both simple and elegant to implement, while remaining robust in practice. The performance of CDC-FM on the ImageNet-1k/256 benchmark under varying $S_{\text{cfg}} \in [1.0, 6.0]$ is reported in Figure 2c and Figure 2d.

Impact of the Diminish Factor. We further investigate the impact of the diminish factor γ in CDC-FM, varying from 1.0 to 5.0 in increments of 0.5, on the ImageNet-1k/256 benchmark. The results, summarized in Figure 2b, reveal that the FID score decreases with increasing γ until a certain tipping point, after which it begins to rise. Meanwhile, the inference time consistently decreases as γ grows and gradually converges.

6 CONCLUSION

We develop a unified multi-stage generation framework based on *stochastic interpolant* with **conditional dependent coupling**, which enables accurate data distribution learning while operating efficiently in pixel space. Moreover, the entire process can be parameterized by a single DiT, thereby achieving end-to-end optimization and facilitating knowledge sharing across stages. We further provide formal proof that the proposed framework significantly reduces the transport cost and inference time. Diverse experiments demonstrate that our method achieves SOTA performance across metrics and is capable of being implemented in higher resolution. Related works, complete Preliminary, Algorithms, Proofs, additional information, and Statement can be seen in the Appendix. The source code will be made publicly available upon acceptance.

ACKNOWLEDGMENTS

This manuscript was co-authored by Oak Ridge National Laboratory (ORNL), operated by UT-Battelle, LLC under Contract No. DE-AC05-00OR22725 with the U.S. Department of Energy. Any subjective views or opinions expressed in this paper do not necessarily represent those of the U.S. Department of Energy or the United States Government.

REFERENCES

Michael S Albergo and Eric Vanden-Eijnden. Building normalizing flows with stochastic interpolants. *arXiv preprint arXiv:2209.15571*, 2022.

Michael S Albergo, Nicholas M Boffi, and Eric Vanden-Eijnden. Stochastic interpolants: A unifying framework for flows and diffusions. *arXiv preprint arXiv:2303.08797*, 2023a.

Michael S Albergo, Mark Goldstein, Nicholas M Boffi, Rajesh Ranganath, and Eric Vanden-Eijnden. Stochastic interpolants with data-dependent couplings. *arXiv preprint arXiv:2310.03725*, 2023b.

Fan Bao, Shen Nie, Kaiwen Xue, Yue Cao, Chongxuan Li, Hang Su, and Jun Zhu. All are worth words: A ViT backbone for diffusion models. In *Proceedings of the IEEE/CVF Conference on Computer Vision and Pattern Recognition (CVPR)*, 2023.

Jean-David Benamou and Yann Brenier. A computational fluid mechanics solution to the monge-kantorovich mass transfer problem. *Numerische Mathematik*, 84(3):375–393, 2000.

Andrew Brock, Jeff Donahue, and Karen Simonyan. Large scale GAN training for high fidelity natural image synthesis. In *International Conference on Learning Representations (ICLR)*, 2019.

Huiwen Chang, Han Zhang, Lu Jiang, Ce Liu, and William T Freeman. Maskgit: Masked generative image transformer. In *Proceedings of the IEEE/CVF conference on computer vision and pattern recognition*, pp. 11315–11325, 2022.

Shuo Chen, Liang Zhang, Rui Wang, et al. Pixelflow: Pixel-space generative models with flow. *arXiv preprint arXiv:2504.07963*, 2025.

Prafulla Dhariwal and Alexander Nichol. Diffusion models beat GANs on image synthesis. In *Advances in Neural Information Processing Systems (NeurIPS)*, 2021.

Alexey Dosovitskiy, Lucas Beyer, Alexander Kolesnikov, Dirk Weissenborn, Xiaohua Zhai, Thomas Unterthiner, Mostafa Dehghani, Matthias Minderer, Georg Heigold, Sylvain Gelly, et al. An image is worth 16x16 words: Transformers for image recognition at scale. *arXiv preprint arXiv:2010.11929*, 2020.

Patrick Esser, Robin Rombach, and Björn Ommer. Taming transformers for high-resolution image synthesis. In *Proceedings of the IEEE/CVF conference on computer vision and pattern recognition*, pp. 12873–12883, 2021a.

Patrick Esser, Robin Rombach, and Björn Ommer. Taming transformers for high-resolution image synthesis. In *Proceedings of the IEEE/CVF Conference on Computer Vision and Pattern Recognition (CVPR)*, 2021b.

Stathi Fotiadis, Noah Brenowitz, Tomas Geffner, Yair Cohen, Michael Pritchard, Arash Vahdat, and Morteza Mardani. Stochastic flow matching for resolving small-scale physics. *arXiv preprint arXiv:2410.19814*, 2024.

Kevin Frans, Danijar Hafner, Sergey Levine, and Pieter Abbeel. One step diffusion via shortcut models. *arXiv preprint arXiv:2410.12557*, 2024.

Zhengyang Geng, Mingyang Deng, Xingjian Bai, J Zico Kolter, and Kaiming He. Mean flows for one-step generative modeling. *arXiv preprint arXiv:2505.13447*, 2025a.

Zhengyang Geng, Ashwini Pokle, Weijian Luo, Justin Lin, and J Zico Kolter. Consistency models made easy. In *The Thirteenth International Conference on Learning Representations*, 2025b.

Irina Higgins, Loic Matthey, Arka Pal, Christopher Burgess, Xavier Glorot, Matthew Botvinick, Shakir Mohamed, and Alexander Lerchner. beta-vae: Learning basic visual concepts with a constrained variational framework. In *International conference on learning representations*, 2017.

Jonathan Ho and Tim Salimans. Classifier-free diffusion guidance. *arXiv preprint arXiv:2207.12598*, 2022.

Jonathan Ho, Chitwan Saharia, William Chan, David J Fleet, Mohammad Norouzi, and Tim Salimans. Cascaded diffusion models for high fidelity image generation. *Journal of Machine Learning Research*, 23(47):1–33, 2022a.

Jonathan Ho, Chitwan Saharia, William Chan, David J. Fleet, Mohammad Norouzi, and Tim Salimans. Cascaded diffusion models for high fidelity image generation. *Journal of Machine Learning Research (JMLR)*, 23(47):1–33, 2022b.

Emiel Hoogeboom, Jonathan Heek, and Tim Salimans. simple diffusion: End-to-end diffusion for high resolution images. In *International Conference on Machine Learning*, pp. 13213–13232. PMLR, 2023.

Emiel Hoogeboom, Thomas Mensink, Jonathan Heek, Kay Lamerigts, Ruiqi Gao, and Tim Salimans. Simpler diffusion (sid2): 1.5 fid on imagenet512 with pixel-space diffusion. In *Proceedings of the IEEE/CVF Conference on Computer Vision and Pattern Recognition (CVPR)*, 2025.

Allan Jabri, David J. Fleet, and Ting Chen. Scalable adaptive computation for iterative generation. *arXiv preprint arXiv:2212.11972*, 2022.

Siyu Jiao, Gengwei Zhang, Yinlong Qian, Jiancheng Huang, Yao Zhao, Humphrey Shi, Lin Ma, Yunchao Wei, and Zequn Jie. Flexvar: Flexible visual autoregressive modeling without residual prediction. *arXiv preprint arXiv:2502.20313*, 2025.

Yang Jin, Zhicheng Sun, Ningyuan Li, Kun Xu, Hao Jiang, Nan Zhuang, Quzhe Huang, Yang Song, Yadong Mu, and Zhouchen Lin. Pyramidal flow matching for efficient video generative modeling. *arXiv preprint arXiv:2410.05954*, 2024.

Minguk Kang, Jun-Yan Zhu, Richard Zhang, Jaesik Park, Eli Shechtman, Sylvain Paris, and Taesung Park. Scaling up GANs for text-to-image synthesis. In *Proceedings of the IEEE/CVF Conference on Computer Vision and Pattern Recognition (CVPR)*, 2023.

Tero Karras, Samuli Laine, and Timo Aila. A style-based generator architecture for generative adversarial networks. In *Proceedings of the IEEE/CVF Conference on Computer Vision and Pattern Recognition (CVPR)*, 2019.

Dongjun Kim, Chieh-Hsin Lai, Wei-Hsiang Liao, Yuhta Takida, Naoki Murata, Toshimitsu Uesaka, Yuki Mitsufuji, and Stefano Ermon. Pagoda: Progressive growing of a one-step generator from a low-resolution diffusion teacher. In *Advances in Neural Information Processing Systems (NeurIPS)*, 2024.

Diederik P Kingma and Max Welling. Auto-encoding variational bayes. *arXiv preprint arXiv:1312.6114*, 2013.

Diederik P. Kingma, Ruiqi Gao, Ben Poole, Jonathan Ho, and Tim Salimans. Understanding diffusion objectives as the ELBO with reparameterized discrete variables. In *Advances in Neural Information Processing Systems (NeurIPS)*, 2023.

Alex Krizhevsky, Ilya Sutskever, and Geoffrey E Hinton. Imagenet classification with deep convolutional neural networks. *Advances in neural information processing systems*, 25, 2012.

Tuomas Kynkänniemi, Miika Aittala, Tero Karras, Samuli Laine, Timo Aila, and Jaakko Lehtinen. Applying guidance in a limited interval improves sample and distribution quality in diffusion models. *Advances in Neural Information Processing Systems*, 37:122458–122483, 2024.

Doyup Lee, Chiheon Kim, Saehoon Kim, Minsu Cho, and Wook-Shin Han. Autoregressive image generation using residual quantization. In *Proceedings of the IEEE/CVF Conference on Computer Vision and Pattern Recognition (CVPR)*, 2022.

Tian Li, Xiaoming Han, Wei Zhang, et al. Fractal generative models. *arXiv preprint arXiv:2502.17437*, 2025.

Tianhong Li, Dina Katabi, and Kaiming He. Self-conditioned image generation via generating representations. *CoRR*, 2023.

Tianhong Li, Yonglong Tian, He Li, Mingyang Deng, and Kaiming He. Autoregressive image generation without vector quantization. *Advances in Neural Information Processing Systems*, 37: 56424–56445, 2024.

Yaron Lipman, Ricky TQ Chen, Heli Ben-Hamu, Maximilian Nickel, and Matt Le. Flow matching for generative modeling. *arXiv preprint arXiv:2210.02747*, 2022.

Yaron Lipman, Marton Havasi, Peter Holderrieth, Neta Shaul, Matt Le, Brian Karrer, Ricky TQ Chen, David Lopez-Paz, Heli Ben-Hamu, and Itai Gat. Flow matching guide and code. *arXiv preprint arXiv:2412.06264*, 2024.

Chenrui Ma, Xi Xiao, Tianyang Wang, and Yanning Shen. Beyond editing pairs: Fine-grained instructional image editing via multi-scale learnable regions, 2025a. URL <https://arxiv.org/abs/2505.19352>.

Chenrui Ma, Rongchang Zhao, Xi Xiao, Hongyang Xie, Tianyang Wang, Xiao Wang, Hao Zhang, and Yanning Shen. Cad-vae: Leveraging correlation-aware latents for comprehensive fair disentanglement. *arXiv preprint arXiv:2503.07938*, 2025b.

Nanye Ma, Mark Goldstein, Michael S. Albergo, Nicholas M. Boffi, Eric Vanden-Eijnden, and Saining Xie. SiT: Exploring flow and diffusion-based generative models with scalable interpolant transformers. In *Proceedings of the European Conference on Computer Vision (ECCV)*, 2024.

James R Norris. *Markov chains*. Number 2. Cambridge university press, 1998.

OpenAI, Josh Achiam, Steven Adler, Sandhini Agarwal, Lama Ahmad, Ilge Akkaya, Florencia Leoni Aleman, Diogo Almeida, Janko Altenschmidt, Sam Altman, Shyamal Anadkat, Red Avila, Igor Babuschkin, Suchir Balaji, Valerie Balcom, Paul Baltescu, Haiming Bao, Mohammad Bavarian, Jeff Belgum, Irwan Bello, Jake Berdine, Gabriel Bernadett-Shapiro, Christopher Berner, Lenny Bogdonoff, Oleg Boiko, Madelaine Boyd, Anna-Luisa Brakman, Greg Brockman, Tim Brooks, Miles Brundage, Kevin Button, Trevor Cai, Rosie Campbell, Andrew Cann, Brittany Carey, Chelsea Carlson, Rory Carmichael, Brooke Chan, Che Chang, Fotis Chantzis, Derek Chen, Sully Chen, Ruby Chen, Jason Chen, Mark Chen, Ben Chess, Chester Cho, Casey Chu, Hyung Won Chung, Dave Cummings, Jeremiah Currier, Yunxing Dai, Cory Decareaux, Thomas Degry, Noah Deutsch, Damien Deville, Arka Dhar, David Dohan, Steve Dowling, Sheila Dunning, Adrien Ecoffet, Atty Eleti, Tyna Eloundou, David Farhi, Liam Fedus, Niko Felix, Simón Posada Fishman, Juston Forte, Isabella Fulford, Leo Gao, Elie Georges, Christian Gibson, Vik Goel, Tarun Gogineni, Gabriel Goh, Rapha Gontijo-Lopes, Jonathan Gordon, Morgan Grafstein, Scott Gray, Ryan Greene, Joshua Gross, Shixiang Shane Gu, Yufei Guo, Chris Halcacy, Jesse Han, Jeff Harris, Yuchen He, Mike Heaton, Johannes Heidecke, Chris Hesse, Alan Hickey, Wade Hickey, Peter Hoeschele, Brandon Houghton, Kenny Hsu, Shengli Hu, Xin Hu, Joost Huizinga, Shantanu Jain, Shawn Jain, Joanne Jang, Angela Jiang, Roger Jiang, Haozhun

Jin, Denny Jin, Shino Jomoto, Billie Jonn, Heewoo Jun, Tomer Kaftan, Łukasz Kaiser, Ali Kamali, Ingmar Kanitscheider, Nitish Shirish Keskar, Tabarak Khan, Logan Kilpatrick, Jong Wook Kim, Christina Kim, Yongjik Kim, Jan Hendrik Kirchner, Jamie Kiros, Matt Knight, Daniel Kokotajlo, Łukasz Kondraciuk, Andrew Kondrich, Aris Konstantinidis, Kyle Kosic, Gretchen Krueger, Vishal Kuo, Michael Lampe, Ikai Lan, Teddy Lee, Jan Leike, Jade Leung, Daniel Levy, Chak Ming Li, Rachel Lim, Molly Lin, Stephanie Lin, Mateusz Litwin, Theresa Lopez, Ryan Lowe, Patricia Lue, Anna Makanju, Kim Malfacini, Sam Manning, Todor Markov, Yaniv Markovski, Bianca Martin, Katie Mayer, Andrew Mayne, Bob McGrew, Scott Mayer McKinney, Christine McLeavey, Paul McMillan, Jake McNeil, David Medina, Aalok Mehta, Jacob Menick, Luke Metz, Andrey Mishchenko, Pamela Mishkin, Vinnie Monaco, Evan Morikawa, Daniel Mossing, Tong Mu, Mira Murati, Oleg Murk, David Mély, Ashvin Nair, Reiichiro Nakano, Rajeev Nayak, Arvind Neelakantan, Richard Ngo, Hyeonwoo Noh, Long Ouyang, Cullen O’Keefe, Jakub Pachocki, Alex Paino, Joe Palermo, Ashley Pantuliano, Giambattista Parascandolo, Joel Parish, Emy Parparita, Alex Passos, Mikhail Pavlov, Andrew Peng, Adam Perelman, Filipe de Avila Belbute Peres, Michael Petrov, Henrique Ponde de Oliveira Pinto, Michael, Pokorny, Michelle Pokrass, Vitchyr H. Pong, Tolly Powell, Alethea Power, Boris Power, Elizabeth Proehl, Raul Puri, Alec Radford, Jack Rae, Aditya Ramesh, Cameron Raymond, Francis Real, Kendra Rimbach, Carl Ross, Bob Rotsted, Henri Roussez, Nick Ryder, Mario Saltarelli, Ted Sanders, Shibani Santurkar, Girish Sastry, Heather Schmidt, David Schnurr, John Schulman, Daniel Sel-sam, Kyla Sheppard, Toki Sherbakov, Jessica Shieh, Sarah Shoker, Pranav Shyam, Szymon Sidor, Eric Sigler, Maddie Simens, Jordan Sitkin, Katarina Slama, Ian Sohl, Benjamin Sokolowsky, Yang Song, Natalie Staudacher, Felipe Petroski Such, Natalie Summers, Ilya Sutskever, Jie Tang, Nikolas Tezak, Madeleine B. Thompson, Phil Tillet, Amin Tootoonchian, Elizabeth Tseng, Preston Tuggle, Nick Turley, Jerry Tworek, Juan Felipe Cerón Uribe, Andrea Vallone, Arun Vijayvergiya, Chelsea Voss, Carroll Wainwright, Justin Jay Wang, Alvin Wang, Ben Wang, Jonathan Ward, Jason Wei, CJ Weinmann, Akila Welihinda, Peter Welinder, Jiayi Weng, Lilian Weng, Matt Wiethoff, Dave Willner, Clemens Winter, Samuel Wolrich, Hannah Wong, Lauren Workman, Sherwin Wu, Jeff Wu, Michael Wu, Kai Xiao, Tao Xu, Sarah Yoo, Kevin Yu, Qiming Yuan, Wojciech Zaremba, Rowan Zellers, Chong Zhang, Marvin Zhang, Shengjia Zhao, Tianhao Zheng, Juntang Zhuang, William Zhuk, and Barret Zoph. Gpt-4 technical report, 2024. URL <https://arxiv.org/abs/2303.08774>.

William Peebles and Saining Xie. Scalable diffusion models with transformers. In *Proceedings of the IEEE/CVF International Conference on Computer Vision (ICCV)*, 2023a.

William Peebles and Saining Xie. Scalable diffusion models with transformers. In *Proceedings of the IEEE/CVF international conference on computer vision*, pp. 4195–4205, 2023b.

Ali Razavi, Aaron van den Oord, and Oriol Vinyals. Generating diverse high-fidelity images with VQ-VAE-2. In *Advances in Neural Information Processing Systems (NeurIPS)*, 2019.

Sucheng Ren, Qihang Yu, Ju He, Xiaohui Shen, Alan Yuille, and Liang-Chieh Chen. Flowar: Scale-wise autoregressive image generation meets flow matching. *arXiv preprint arXiv:2412.15205*, 2024.

Sucheng Ren, Qihang Yu, Ju He, Xiaohui Shen, Alan Yuille, and Liang-Chieh Chen. Flowar: Scale-wise autoregressive image generation meets flow matching. In *Forty-second International Conference on Machine Learning*, 2025.

Robin Rombach, Andreas Blattmann, Dominik Lorenz, Patrick Esser, and Björn Ommer. High-resolution image synthesis with latent diffusion models. In *Proceedings of the IEEE/CVF Conference on Computer Vision and Pattern Recognition (CVPR)*, 2022.

Yang Song, Prafulla Dhariwal, Mark Chen, and Ilya Sutskever. Consistency models. 2023.

Peng Sun, Daquan Zhou, Xudong Wang, Zheng Chen, et al. Autoregressive model beats diffusion: Llama for scalable image generation. *arXiv preprint arXiv:2406.06525*, 2024.

Keyu Tian, Yi Jiang, Zehuan Yuan, Bingyue Peng, and Liwei Wang. Visual autoregressive modeling: Scalable image generation via next-scale prediction. *Advances in neural information processing systems*, 37:84839–84865, 2024a.

Keyu Tian, Linjiang Sun, Tianhe Zhang, Dahua Lin, et al. Scalable image generation via next-scale prediction. In *Advances in Neural Information Processing Systems (NeurIPS)*, 2024b.

Michael Tschannen, André Susano Pinto, and Alexander Kolesnikov. Jetformer: An autoregressive generative model of raw images and text. *arXiv preprint arXiv:2411.19722*, 2024.

Ashish Vaswani, Noam Shazeer, Niki Parmar, Jakob Uszkoreit, Llion Jones, Aidan N Gomez, Łukasz Kaiser, and Illia Polosukhin. Attention is all you need. *Advances in neural information processing systems*, 30, 2017.

Cédric Villani. *Topics in optimal transportation*, volume 58. American Mathematical Soc., 2021.

Cédric Villani et al. *Optimal transport: old and new*, volume 338. Springer, 2008.

Xi Xiao, Yunbei Zhang, Xingjian Li, Tianyang Wang, Xiao Wang, Yuxiang Wei, Jihun Hamm, and Min Xu. Visual instance-aware prompt tuning, 2025a. URL <https://arxiv.org/abs/2507.07796>.

Xi Xiao, Yunbei Zhang, Yanshuh Li, Xingjian Li, Tianyang Wang, Jihun Hamm, Xiao Wang, and Min Xu. Visual variational autoencoder prompt tuning, 2025b. URL <https://arxiv.org/abs/2503.17650>.

Xi Xiao, Yunbei Zhang, Janet Wang, Lin Zhao, Yuxiang Wei, Hengjia Li, Yanshu Li, Xiao Wang, Swalpa Kumar Roy, Hao Xu, and Tianyang Wang. Roadbench: A vision-language foundation model and benchmark for road damage understanding, 2025c. URL <https://arxiv.org/abs/2507.17353>.

H Yan, X Liu, J Pan, JH Liew, Q Liu, and J Feng. Perflow: Piecewise rectified flow as universal plug-and-play accelerator. *arXiv preprint arXiv:2405.07510*, 2024.

Jiahui Yu, Xin Li, Jing Yu Koh, Han Zhang, Ruoming Pang, James Qin, Alexander Ku, Yuanzhong Xu, Jason Baldridge, and Yonghui Wu. Vector-quantized image modeling with improved vqgan. *arXiv preprint arXiv:2110.04627*, 2021.

Lijun Yu, Jose Lezama, Nitesh Bharadwaj Gundavarapu, Luca Versari, Kihyuk Sohn, David Minnen, Yong Cheng, Agrim Gupta, Xiuye Gu, Alexander G Hauptmann, et al. Language model beats diffusion-tokenizer is key to visual generation. In *The Twelfth International Conference on Learning Representations*, 2025.

APPENDIX CONTENTS

A Related Works	15
B Qualitative results	16
C Stochastic Interpolant	16
D Proof	18
D.1 Proof of Theorem 2	18
D.1.1 Problem Formulation and Definitions	18
D.1.2 Orthogonal Decomposition of Image Energy	19
D.1.3 Analysis of Transportation Costs	20
D.1.4 Main Proof and Conclusion	21
D.2 Proof of Theorem 3	22
D.2.1 Problem Formulation and Assumptions	22
D.2.2 Analysis of Computational Load	23
D.2.3 Main Proof and Conclusion	23
E Algorithm	24
F Classifier-Free Guidance for Conditional Dependent Coupling	24
G Implement Details	28

A RELATED WORKS

Latent Space Generation. Variational Autoencoders (VAEs) Kingma & Welling (2013); Higgins et al. (2017); Ma et al. (2025b) enable generative models to perform Flow/Diffusion generation, as well as autoregressive generation, within a lower-dimensional latent space Rombach et al. (2022); Peebles & Xie (2023a); Ma et al. (2024); Razavi et al. (2019); Esser et al. (2021b); Yu et al. (2021); Lee et al. (2022); Sun et al. (2024); Ren et al. (2024); Tian et al. (2024b); Jabri et al. (2022). This leads to more efficient training and inference. However, the compact representations produced by the encoder and the subsequent decoding process inevitably introduce a degree of information and detail loss Li et al. (2024); Hoogeboom et al. (2025; 2023); Xiao et al. (2025a;b); Ma et al. (2025a). Despite this limitation, VAEs remain a crucial component in these generative models. Moreover, they typically cannot be trained jointly with the generative model in a fully end-to-end manner Chen et al. (2025).

Pixel Space Generation. Although directly implementing the generation process avoids the need for VAEs and facilitates the preservation of fine-grained details, it is highly inefficient for both training and inference Rombach et al. (2022); Hoogeboom et al. (2025; 2023); Bao et al. (2023). Furthermore, due to the high dimensionality and complexity of the data distribution, learning to generate samples that faithfully capture detailed information from the target distribution becomes particu-

larly challenging, especially in the absence of VAEs to extract meaningful latent features Chen et al. (2025); Jin et al. (2024); Ren et al. (2024); Tian et al. (2024b); Jabri et al. (2022); Sun et al. (2024).

Multi-stage Generation. Multi-stage generation methods advance sample synthesis by decomposing the process into a sequence of stages, where early stages operate in a lower-dimensional space to improve efficiency Chen et al. (2025); Jin et al. (2024); Tian et al. (2024b); Jiao et al. (2025); Ren et al. (2025); Ho et al. (2022b); Jabri et al. (2022); Xiao et al. (2025c); Ma et al. (2025a). In addition, the overall generative task is divided into subtasks at each stage, enabling the model to gradually capture the complexity of the target data distribution Tian et al. (2024b); Jiao et al. (2025); Ren et al. (2025); Ho et al. (2022b). However, the use of disentangled stage designs hinders unified model parameterization and end-to-end optimization Chen et al. (2025); Jin et al. (2024). Furthermore, the decoupling inherent in multi-stage frameworks may lead to inaccurate modeling of the data distribution, thereby introducing errors that can accumulate across stages Chen et al. (2025); Jin et al. (2024).

B QUALITATIVE RESULTS

We visualize the class-conditional image generation result of our method in Figure 3, demonstrating high-fidelity, accuracy, and diversity across all the classes.

C STOCHASTIC INTERPOLANT

The stochastic interpolant unifies the theory of Ordinary Differential Equations (ODEs) and Stochastic Differential Equations (SDEs).

Definition 3 (Stochastic Interpolant). Albergo et al. (2023a;b); Albergo & Vanden-Eijnden (2022) Given two probability density functions $\rho_0, \rho_1 : \mathbb{R}^d \rightarrow \mathbb{R}_{\geq 0}$, a stochastic interpolant between ρ_0 and ρ_1 is a stochastic process I_t defined as

$$I_t = \alpha_t x_0 + \beta_t x_1 + \gamma_t z, \quad t \in [0, 1] \quad (22)$$

where α_t , β_t , and γ_t^2 are differentiable functions of time satisfying the boundary conditions

$$\alpha_0 = \beta_1 = 1, \quad \alpha_1 = \beta_0 = \gamma_0 = \gamma_1 = 0, \quad \text{and} \quad \alpha_t^2 + \beta_t^2 + \gamma_t^2 > 0 \quad \forall t \in [0, 1].$$

The pair (x_0, x_1) is drawn from a joint probability density $\rho(x_0, x_1)$ with finite second moments, whose marginals are ρ_0 and ρ_1 :

$$\int_{\mathbb{R}^d} \rho(x_0, x_1) dx_1 = \rho_0(x_0), \quad (23)$$

$$\int_{\mathbb{R}^d} \rho(x_0, x_1) dx_0 = \rho_1(x_1), \quad (24)$$

and $z \sim \mathcal{N}(0, \text{Id})$ a Gaussian random variable independent of (x_0, x_1) , i.e., $z \perp (x_0, x_1)$.

The stochastic interpolant framework uses information about the process I_t to derive either an ODE or an SDE. The solutions X_t to these equations are designed to push the initial law ρ_0 onto the law of the interpolant I_t for all times $t \in [0, 1]$. Consequently, the process I_t satisfies $I_{t=0} = x_0 \sim \rho_0(x_0)$ and $I_{t=1} = x_1 \sim \rho_1(x_1)$. This property allows for generative modeling: by drawing samples $x_0 \sim \rho_0(x_0)$ and using them as initial conditions $X_{t=0} = x_0$, one can generate samples $X_{t=1} \sim \rho_1(x_1)$ via numerical integration of the corresponding ODE or SDE.

Theorem 4 (Transport equation). *Let the time-dependent density of the stochastic interpolant I_t be $\rho_t(x)$. We define the velocity field $b_t(x)$ and the score field $s_t(x)$ as:*

$$b_t(x) = \mathbb{E}[\dot{I}_t \mid I_t = x] \quad (25)$$

$$s_t(x) = \nabla \log \rho_t(x) \quad (26)$$

where the dot denotes the time-derivative: $\dot{f} = \frac{df}{dt}$ and the expectation is over $\rho(x_0, x_1)$ and z conditional on $I_t = x$. The probability density $\rho_t(x)$ satisfies the boundary conditions $\rho_{t=0}(x) = \rho_0(x)$ and $\rho_{t=1}(x) = \rho_1(x)$, and solves the transport equation:

$$\partial_t \rho_t(x) + \nabla \cdot (b_t(x) \rho_t(x)) = 0. \quad (27)$$



Figure 3: ImageNet-1k/256 class-conditional generation results.

Moreover, for every t such that $\gamma_t \neq 0$, the score is given by:

$$s_t(x) = -\gamma_t^{-1} \mathbb{E}(z \mid I_t = x). \quad (28)$$

Finally, the fields b_t and s_t are the unique minimizers of the respective objective functions:

$$L_b(\hat{b}) = \int_0^1 \mathbb{E} \left[\left| \hat{b}_t(I_t) \right|^2 - 2\hat{I}_t \cdot \hat{b}_t(I_t) \right] dt, \quad (29)$$

$$L_s(\hat{s}) = \int_0^1 \mathbb{E} \left[\left| \hat{s}_t(I_t) \right|^2 + 2\gamma_t^{-1} z \cdot \hat{s}_t(I_t) \right] dt, \quad (30)$$

where \mathbb{E} denotes an expectation over $(x_0, x_1) \sim \rho(x_0, x_1)$ and $z \sim \mathcal{N}(0, \text{Id})$.

The objective functions equation 29 and equation 30 can be readily estimated in practice from samples $(x_0, x_1) \sim \rho(x_0, x_1)$ and $z \sim \mathcal{N}(0, 1)$, which will enable us to learn approximations for use in a generative model. The transport equation 27 can be used to derive generative models, as we now show.

Corollary 2 (Probability flow (ODE) and diffusions (SDE)). *The transport equation 27 implies that the density of the solutions X_t to the probability flow ODE matches the interpolant density ρ_t . The solutions to the probability flow equation:*

$$\dot{X}_t = b_t(X_t) \quad (31)$$

satisfy the properties that

$$X_{t=1} \sim \rho_1(x_1) \quad \text{if} \quad X_{t=0} \sim \rho_0(x_0), \quad (32)$$

$$X_{t=0} \sim \rho_0(x_0) \quad \text{if} \quad X_{t=1} \sim \rho_1(x_1). \quad (33)$$

In addition, for any choice of a time-dependent diffusion coefficient $\epsilon_t \geq 0$, solutions to the forward SDE

$$dX_t^F = (b_t(X_t^F) + \epsilon_t s_t(X_t^F)) dt + \sqrt{2\epsilon_t} dW_t, \quad (34)$$

satisfy the property that

$$X_{t=1}^F \sim \rho_1(x_1) \quad \text{if} \quad X_{t=0}^F \sim \rho_0(x_0). \quad (35)$$

And solutions to the backward SDE

$$dX_t^R = (b_t(X_t^R) - \epsilon_t s_t(X_t^R)) dt + \sqrt{2\epsilon_t} dW_t, \quad (36)$$

satisfy the property that

$$X_{t=0}^R \sim \rho_0(x_0) \quad \text{if} \quad X_{t=1}^R \sim \rho_1(x_1). \quad (37)$$

Both deterministic and stochastic generative models were derived within the stochastic interpolant framework.

D PROOF

D.1 PROOF OF THEOREM 2

We provide a formal proof that a cascaded image generation model using Flow Matching with **conditional dependent coupling** has a significantly lower transportation cost than a direct, single-stage model that generates a high-resolution image from Gaussian noise, as shown in Theorem 2. The proof is based on an orthogonal decomposition of the image signal energy, which reveals that the cost difference is primarily driven by the dimensionality of the initial noise space.

D.1.1 PROBLEM FORMULATION AND DEFINITIONS

Our goal is to prove that the transportation cost of a direct Flow Matching model (L_A) is greater than the total transport cost of a multi-stage cascaded model with conditional dependent couplings (L_B).

Proposition 1 (Transportation Cost Bound). *From Definition 2, the transportation cost of a probability flow is bounded by the integral of the expected squared norm of the interpolant's time derivative. For an interpolant path from a source distribution $\rho_0(x_0)$ to a target distribution $\rho_1(x_1)$, we denote this bound as L :*

$$\text{Cost} = \mathbb{E}_{x_0 \sim \rho_0} [|X_{t=1}(x_0) - x_0|^2] \leq \int_0^1 \mathbb{E} [|\dot{I}_t|^2] dt := L. \quad (38)$$

For simplicity in the proof, we analyze the case where the interpolant is $I_t = (1 - t)x_0 + tx_1$, such that its derivative is $\dot{I}_t = x_1 - x_0$. The logic holds for general interpolants. In this case, the cost bound reduces to Lipman et al. (2024); Albergo et al. (2023b):

$$L = \mathbb{E}[|x_1 - x_0|^2]. \quad (39)$$

Model A: Direct Generation This model generates a high-resolution image $x^{(K)} \in \mathbb{R}^{d_K}$ in a single stage.

- **Source Distribution** $\rho_0(x_0)$: $x_0 \sim \mathcal{N}(0, \sigma^2 I_{d_K})$.
- **Target Distribution** $\rho_1(x_1)$: The high-resolution data distribution, $x_1 \sim x^{(K)}$.
- **Cost** (L_A): The transport cost from x_0 to x_1 .

Model B: Cascaded Generation This model generates the image in K stages, from resolution d_1 to d_K .

- **Stage 1:** Generates a low-resolution image $x_1^{(1)} \in \mathbb{R}^{d_1}$.
 - Source: $x_0^{(1)} \sim \mathcal{N}(0, \sigma^2 I_{d_1})$.
 - Target: $x_1^{(1)} \sim \rho_1^{(1)}(x_1^{(1)} | x^{(K)})$.
 - Cost: L_1 .
- **Stages $k \in [2, K]$:** Refines a coarse image to a higher resolution image $x_1^{(k)} \in \mathbb{R}^{d_k}$.
 - Target: $x_1^{(k)} \sim \rho_1^{(k)}(x_1^{(k)} | x^{(K)})$.
 - Source: $x_0^{(k)} \sim \rho_0^{(k)}(x_0^{(k)} | x_1^{(k)})$ is defined by a deterministic **conditional dependent coupling** with a small stage-dependent Gaussian noise: $x_0^{(k)} = U_k(D_k(x_1^{(k)})) + \sigma_k \zeta_k$, as shown in equation 9.
 - Cost: L_k .
- **Total Cost** (L_B): The sum of the costs of all stages, $L_B = \sum_{k=1}^K L_k$.

We seek to prove that $L_A > L_B$.

D.1.2 ORTHOGONAL DECOMPOSITION OF IMAGE ENERGY

We formalize the concept that an image can be represented as a base layer plus a sum of details.

Definition 4 (Multiresolution Projections). Let the vector space be that of the highest resolution, \mathbb{R}^{d_K} . We define an embedding operator $U_{k \rightarrow K} : \mathbb{R}^{d_k} \rightarrow \mathbb{R}^{d_K}$ that upscales a level- k image to the full resolution space. We then define a projection operator $D_{K \rightarrow k} : \mathbb{R}^{d_K} \rightarrow \mathbb{R}^{d_k}$ that projects a high-resolution image onto the subspace of images with resolution k . These two definitions are inherited from the previous section. For an image $x \in \mathbb{R}^{d_K}$, let $\tilde{x}^{(k)} = U_{k \rightarrow K}(D_{K \rightarrow k}(x))$. We also define the null image $\tilde{x}^{(0)} = \mathbf{0}$. Let the **detail vector** at level k be $\tilde{\epsilon}^{(k)} = \tilde{x}^{(k)} - \tilde{x}^{(k-1)}$.

Assumption 1 (Orthogonality of Details). The detail vector $\tilde{\epsilon}^{(k)}$, which contains the frequency content for level k , is orthogonal to the detail vectors of all other levels.

$$\mathbb{E}[(\tilde{\epsilon}^{(k)})^T \tilde{\epsilon}^{(j)}] = 0 \quad \text{for } k \neq j \quad (40)$$

This also reflects the nature of the process, in which each stage responsible for adding details is conditionally independent, as illustrated in equation 14. Under Assumption 1, the full image can be written as a telescoping sum:

$$x = \tilde{x}^{(K)} = \sum_{k=1}^K (\tilde{x}^{(k)} - \tilde{x}^{(k-1)}) = \sum_{k=1}^K \tilde{\epsilon}^{(k)} \quad (41)$$

Lemma 1 (Energy Decomposition). *Under Assumption 1, the expected energy of an image is the sum of the expected energies of its orthogonal detail components.*

$$\mathbb{E}[|x|^2] = \mathbb{E} \left[\left| \sum_{k=1}^K \tilde{\epsilon}^{(k)} \right|^2 \right] = \sum_{k=1}^K \mathbb{E}[|\tilde{\epsilon}^{(k)}|^2] \quad (42)$$

Proof. This follows directly from the linearity of expectation and the orthogonality assumption, as all cross-terms $\mathbb{E}[(\tilde{\epsilon}^{(k)})^T \tilde{\epsilon}^{(j)}]$ for $k \neq j$ vanish. \square

D.1.3 ANALYSIS OF TRANSPORTATION COSTS

Cost of the Direct Model (L_A). The cost is $L_A = \mathbb{E}[|x_1 - x_0|^2]$, where $x_1 \sim x^{(K)}$ and $x_0 \sim \mathcal{N}(0, \sigma^2 I_{d_K})$. Due to independence and $\mathbb{E}[x_0] = 0$:

$$\begin{aligned} L_A &= \mathbb{E}[|x_1|^2] - 2\mathbb{E}[x_1^T x_0] + \mathbb{E}[|x_0|^2] \\ &= \mathbb{E}[|x_1|^2] + \mathbb{E}[|x_0|^2] \end{aligned} \quad (43)$$

Using Lemma 1 and the variance of the noise, $\mathbb{E}[|x_0|^2] = d_K \sigma^2$:

$$L_A = \left(\sum_{k=1}^K \mathbb{E}[|\tilde{\epsilon}^{(k)}|^2] \right) + d_K \sigma^2 \quad (44)$$

Cost of the Cascaded Model with conditional dependent couplings (L_B). The total cost is $L_B = \sum_{k=1}^K L_k$.

- **Stage 1:** $L_1 = \mathbb{E}[|x_1^{(1)} - x_0^{(1)}|^2] = \mathbb{E}[|x_1^{(1)}|^2] + \mathbb{E}[|x_0^{(1)}|^2]$. The data $x_1^{(1)}$ represents the coarsest level of detail, corresponding to $\tilde{\epsilon}^{(1)}$. The noise variance is $\mathbb{E}[|x_0^{(1)}|^2] = d_1 \sigma^2$. Thus,

$$L_1 \approx \mathbb{E}[|\tilde{\epsilon}^{(1)}|^2] + d_1 \sigma^2 \quad (45)$$

- **Stages $k \in [2, K]$:** The cost is $L_k = \mathbb{E}[|x_1^{(k)} - x_0^{(k)}|^2]$. Substituting the data-dependent coupling $x_0^{(k)} = U_k(D_k(x_1^{(k)})) + \sigma_k \zeta_k$, we get:

$$\begin{aligned} L_k &= \mathbb{E}[|x_1^{(k)} - U_k(D_k(x_1^{(k)})) - \sigma_k \zeta_k|^2] \\ &= \mathbb{E}[|x_1^{(k)} - U_k(D_k(x_1^{(k)}))|^2] - 2 \mathbb{E}[\sigma_k \zeta_k^T \cdot (x_1^{(k)} - U_k(D_k(x_1^{(k)})))^T] + \mathbb{E}[|\sigma_k \zeta_k|^2] \\ &= \mathbb{E}[|x_1^{(k)} - U_k(D_k(x_1^{(k)}))|^2] - 2 \mathbb{E}[\sigma_k \zeta_k] \mathbb{E}[(x_1^{(k)} - U_k(D_k(x_1^{(k)})))^T] + \mathbb{E}[|\sigma_k \zeta_k|^2] \\ &= \mathbb{E}[|x_1^{(k)} - U_k(D_k(x_1^{(k)}))|^2] + \mathbb{E}[|\sigma_k \zeta_k|^2], \end{aligned} \quad (46)$$

where independence: $\sigma_k \zeta_k \perp\!\!\!\perp (x_1^{(k)} - U_k(D_k(x_1^{(k)})))$ and $\mathbb{E}[\sigma_k \zeta_k] = 0$. $\mathbb{E}[|x_1^{(k)} - U_k(D_k(x_1^{(k)}))|^2]$ is the expected energy of the details required to go from resolution $k-1$ to k , which corresponds precisely to the energy of the detail vector $\tilde{\epsilon}^{(k)}$: $\mathbb{E}[|\tilde{\epsilon}^{(k)}|^2]$, and the variance of the noise, $\mathbb{E}[|\sigma_k \zeta_k|^2] = d_k \sigma_k^2$:

$$L_k \approx \mathbb{E}[|\tilde{\epsilon}^{(k)}|^2] + d_k \sigma_k^2 \quad (47)$$

Summing the costs for all stages of Model B:

$$\begin{aligned} L_B &= L_1 + \sum_{k=2}^K L_k \\ &\approx (\mathbb{E}[|\tilde{\epsilon}^{(1)}|^2] + d_1 \sigma^2) + \sum_{k=2}^K \left(\mathbb{E}[|\tilde{\epsilon}^{(k)}|^2] + d_k \sigma_k^2 \right) \\ &= \left(\sum_{k=1}^K \mathbb{E}[|\tilde{\epsilon}^{(k)}|^2] \right) + d_1 \sigma^2 + \left(\sum_{k=2}^K d_k \sigma_k^2 \right), \end{aligned} \quad (48)$$

Here, $d_k = 2^{k-1} d_1$ for $1 \leq k \leq K$, reflecting the pyramid structure that aligns with the conditional dependent coupling design. As discussed in the previous section, we define σ_k to decrease as k increases, which matches the intuition that as the stage k progresses, the requirements for diversity and stochasticity gradually diminish, as shown in equation 20, where we specify $\gamma = 2$ for simplicity:

$$\sigma_k = 2^{-(k-1)} \sigma \quad \text{for } 2 \leq k \leq K. \quad (49)$$

D.1.4 MAIN PROOF AND CONCLUSION

Proof. From the detailed analysis in the previous subsections, we have derived the transportation costs for the direct and cascaded models:

$$L_A = \left(\sum_{k=1}^K \mathbb{E}[|\tilde{\epsilon}^{(k)}|^2] \right) + d_K \sigma^2, \quad (50)$$

where d_K is the dimensionality of the high-resolution image space.

For the cascaded model with K stages, the total cost is the sum of the costs of all stages:

$$L_B = \left(\sum_{k=1}^K \mathbb{E}[|\tilde{\epsilon}^{(k)}|^2] \right) + d_1 \sigma^2 + \sum_{k=2}^K d_k \sigma_k^2. \quad (51)$$

The term $\sum_{k=1}^K \mathbb{E}[|\tilde{\epsilon}^{(k)}|^2]$, representing the total signal energy (see Lemma 1), appears in both L_A and L_B and thus cancels when we consider the difference:

$$L_A - L_B = d_K \sigma^2 - \left(d_1 \sigma^2 + \sum_{k=2}^K d_k \sigma_k^2 \right). \quad (52)$$

To evaluate the sign of $L_A - L_B$, we use the definitions of d_k and σ_k from the cascaded model with conditional dependent coupling:

$$d_k = 2^{k-1} d_1, \quad \sigma_k = 2^{-(k-1)} \sigma \quad \text{for } 2 \leq k \leq K.$$

Thus, the second term can be expanded as:

$$\sum_{k=2}^K d_k \sigma_k^2 = \sum_{k=2}^K (2^{k-1} d_1) (2^{-(k-1)} \sigma)^2 = d_1 \sigma^2 \sum_{k=2}^K 2^{-(k-1)}. \quad (53)$$

We have:

$$L_A - L_B = \sigma^2 \left(d_K - d_1 - d_1 \sum_{k=2}^K 2^{-(k-1)} \right). \quad (54)$$

Since $d_K = 2^{K-1} d_1$, we obtain:

$$L_A - L_B = \sigma^2 d_1 \left(2^{K-1} - 1 - \sum_{k=2}^K 2^{-(k-1)} \right). \quad (55)$$

Specifically, $L_A - L_B = 0$ when $K = 1$. Observe that $2^{K-1} - 1 \gg \sum_{k=2}^K 2^{-(k-1)}$ for all $K \geq 2$, because the left-hand side grows exponentially while the right-hand side is a bounded geometric series:

$$\sum_{k=2}^K 2^{-(k-1)} < \sum_{m=1}^{\infty} 2^{-m} = 1.$$

Therefore, the term in parentheses is strictly positive:

$$2^{K-1} - 1 - \sum_{k=2}^K 2^{-(k-1)} > 0.$$

Since $\sigma^2 > 0$ and $d_1 > 0$, we conclude:

$$L_A - L_B > 0 \implies L_A > L_B. \quad (56)$$

This completes the proof. The main factor leading to $L_A > L_B$ is that the direct model pays the cost of transporting a high-dimensional Gaussian noise vector of dimension d_K , while the cascaded model introduces noise primarily in the low-dimensional early stages and relies on conditional dependent couplings to incrementally add fine-grained details. This multi-resolution structure results in a strictly lower total transportation cost. \square

□

D.2 PROOF OF THEOREM 3

We provide a formal proof that the cascaded Flow Matching model with the **conditional dependent coupling** strategy has strictly smaller expected inference time than the naive single-stage model for high-resolution image generation, as stated in Theorem 3. The argument follows three steps: (i) relate the expected inference-time functional $\iota(\cdot)$ to the Number of Function Evaluations (NFE) and the per-evaluation cost, (ii) connect NFE to a transportation cost, and (iii) compare the resulting computational “loads” of the direct and cascaded schemes by separating signal and noise contributions.

D.2.1 PROBLEM FORMULATION AND ASSUMPTIONS

Recall the theorem’s notation:

$$T_A = \mathbb{E}[\iota(x_0 \rightarrow \hat{x}_1)], \quad T_B = \sum_{k=1}^K \mathbb{E}[\iota(x_0^{(k)} \rightarrow \hat{x}_1^{(k)})].$$

The direct model draws $x_0 \sim \mathcal{N}(0, \sigma^2 I_{d_K})$ and produces $\hat{x}_1 \in \mathbb{R}^{d_K}$ in one stage; the cascaded model comprises K stages, with stage k transporting $x_0^{(k)} \sim \mathcal{N}(x_0^{(k)}; m_k(x_1^{(k)}), \sigma_k^2 I_{d_k})$ to $\hat{x}_1^{(k)} \in \mathbb{R}^{d_k}$, where $d_1 < \dots < d_K$, as state in equation 10.

Per-evaluation cost model. For ODE-based generators (e.g., probability flow ODEs), the expected inference-time cost is the product of the NFE and the cost per function evaluation. With a fixed backbone and solver tolerance, the per-evaluation cost scales linearly with the ambient dimensionality:

$$\mathbb{E}[\iota(x_0 \rightarrow \hat{x}_1)] = \alpha N_A d_K, \quad \mathbb{E}[\iota(x_0^{(k)} \rightarrow \hat{x}_1^{(k)})] = \alpha N_k d_k,$$

for some constant $\alpha > 0$. Hence

$$T_A = \alpha N_A d_K, \quad T_B = \alpha \sum_{k=1}^K N_k d_k.$$

To prove $T_A > T_B$ it suffices to show

$$\sum_{k=1}^K N_k d_k < N_A d_K. \quad (57)$$

Assumption 2 (NFE vs. Transportation Cost). The NFE required to solve a probability flow ODE to a given accuracy is proportional to the transportation cost $L = \mathbb{E}[|x_1 - x_0|^2]$. This cost serves as a proxy for the complexity of the vector field.

$$N_i = C \cdot L_i \quad (58)$$

where C is a constant dependent on the ODE solver and desired precision.

Under this assumption, equation 57 is equivalent to

$$\sum_{k=1}^K L_k d_k < L_A d_K. \quad (59)$$

Define the *computational load* of a transport as $\text{Load} := L \times d$. Then

$$\text{Load}_A = L_A d_K, \quad \text{Load}_B = \sum_{k=1}^K L_k d_k,$$

and proving equation 59 is equivalent to showing $\text{Load}_B < \text{Load}_A$.

D.2.2 ANALYSIS OF COMPUTATIONAL LOAD

We use the transportation-cost decompositions established in Section D.1. Writing $\tilde{\epsilon}^{(k)}$ for the signal component associated with scale/stage k :

Direct model (single stage). The load is the product of its transportation cost L_A (equation 50) and the dimensionality of the final image d_K .

$$\begin{aligned} \text{Load}_A &= L_A \cdot d_K \\ &= \left(\left(\sum_{j=1}^K \mathbb{E}[|\tilde{\epsilon}^{(j)}|^2] \right) + d_K \sigma^2 \right) d_K \\ &= d_K \sum_{j=1}^K \mathbb{E}[|\tilde{\epsilon}^{(j)}|^2] + d_K^2 \sigma^2 \end{aligned} \quad (60)$$

Cascaded model (multi-stage). The total load is the sum of the loads of each stage, where the load for stage k is $L_k \cdot d_k$, where L_k is shown in equation 47. For stage 1, $x_0^{(1)} \sim \mathcal{N}(0, \sigma^2 I_{d_1})$; for stages $k \geq 2$, the conditional dependent coupling strategy injects $x_0^{(k)} \sim \mathcal{N}(x_0^{(k)}; m_k(x_1^{(k)}), \sigma_k^2 I_{d_k})$. Hence

$$\begin{aligned} \text{Load}_B &= \sum_{k=1}^K L_k d_k = L_1 d_1 + \sum_{k=2}^K L_k d_k \\ &= (\mathbb{E}[|\tilde{\epsilon}^{(1)}|^2] + d_1 \sigma^2) d_1 + \sum_{k=2}^K (\mathbb{E}[|\tilde{\epsilon}^{(k)}|^2] + d_k \sigma_k^2) d_k \\ &= \mathbb{E}[|\tilde{\epsilon}^{(1)}|^2] d_1 + d_1^2 \sigma^2 + \sum_{k=2}^K \mathbb{E}[|\tilde{\epsilon}^{(k)}|^2] d_k + \sum_{k=2}^K d_k^2 \sigma_k^2 \\ &= \left(\sum_{k=1}^K \mathbb{E}[|\tilde{\epsilon}^{(k)}|^2] d_k \right) + \left(d_1^2 \sigma^2 + \sum_{k=2}^K d_k^2 \sigma_k^2 \right) \end{aligned} \quad (61)$$

D.2.3 MAIN PROOF AND CONCLUSION

We compare equation 60 and equation 61 by splitting into signal and noise parts.

(1) Signal component. From equation 60 and equation 61,

$$\text{Load}_{A,\text{signal}} = d_K \sum_{k=1}^K \mathbb{E}[|\tilde{\epsilon}^{(k)}|^2], \quad \text{Load}_{B,\text{signal}} = \sum_{k=1}^K \mathbb{E}[|\tilde{\epsilon}^{(k)}|^2] d_k.$$

Since $d_k < d_K$ for all $1 \leq k < K$, each term in the summation for $\text{Load}_{B,\text{signal}}$ is smaller than (or equal to, when $k = K$) the corresponding term for $\text{Load}_{A,\text{signal}}$. Therefore:

$$\sum_{k=1}^K \mathbb{E}[|\tilde{\epsilon}^{(k)}|^2] d_k < d_K \sum_{k=1}^K \mathbb{E}[|\tilde{\epsilon}^{(k)}|^2] \quad (62)$$

The computational work related to generating the image content is strictly lower in the cascaded model because most detail components $\tilde{\epsilon}^{(k)}$ are processed at much lower dimensionalities d_k .

(2) Noise component (coupling strategy). Adopt the conditional dependent coupling in which spatial resolutions double by stage and the injected noise variance is inversely scaled, as shown in equation 20:

$$d_k = 2^{k-1} d_1, \quad \sigma_k = 2^{-(k-1)} \sigma \quad \text{for } 2 \leq k \leq K.$$

Then

$$\begin{aligned}
\text{Load}_{B,\text{noise}} &= d_1^2 \sigma^2 + \sum_{k=2}^K d_k^2 \sigma_k^2 \\
&= d_1^2 \sigma^2 + \sum_{k=2}^K (2^{k-1} d_1)^2 (2^{-(k-1)} \sigma)^2 \\
&= d_1^2 \sigma^2 + \sum_{k=2}^K (2^{2(k-1)} d_1^2) (2^{-2(k-1)} \sigma^2) \\
&= d_1^2 \sigma^2 + \sum_{k=2}^K d_1^2 \sigma^2 \\
&= d_1^2 \sigma^2 + (K-1) d_1^2 \sigma^2 = K d_1^2 \sigma^2,
\end{aligned} \tag{63}$$

whereas for the direct model

$$\text{Load}_{A,\text{noise}} = d_K^2 \sigma^2 = (2^{K-1} d_1)^2 \sigma^2 = 2^{2(K-1)} d_1^2 \sigma^2 \tag{64}$$

For $K = 1$, both loads coincide; for any practical cascade with $K \geq 2$,

$$\text{Load}_{B,\text{noise}} = K d_1^2 \sigma^2 < 2^{2(K-1)} d_1^2 \sigma^2 = \text{Load}_{A,\text{noise}}. \tag{65}$$

Thus the noise-related work is exponentially smaller in the cascaded scheme.

Combining (1) and (2). Adding equation 62 and equation 65 yields

$$\text{Load}_B < \text{Load}_A \iff \sum_{k=1}^K L_k d_k < L_A d_K.$$

Using the NFE-transportation-cost proportionality and the per-evaluation cost model, common multiplicative constants cancel, giving

$$T_B = \sum_{k=1}^K \mathbb{E}[\iota(x_0^{(k)} \rightarrow \hat{x}_1^{(k)})] < \mathbb{E}[\iota(x_0 \rightarrow \hat{x}_1)] = T_A.$$

For $K = 1$ the two procedures coincide, while for every $K \geq 2$ the inequality is strict. This completes the proof of Theorem 3.

E ALGORITHM

Here we present the detailed unconditional training and inference procedures for the unified multi-stage generative model b^θ with **conditional dependent coupling** in Algorithm 1 and Algorithm 2. The inference steps are described using the forward Euler method Lipman et al. (2024; 2022) for solving the ODE, as a simple example of a numerical solver.

F CLASSIFIER-FREE GUIDANCE FOR CONDITIONAL DEPENDENT COUPLING

Rationale. Because each stage k in our multi-stage model learns the *accurate* data distribution $\rho_1^{(k)}(x_1^{(k)} \mid x^{(K)})$ under the **conditional dependent coupling** (Sec. 3.3), Classifier-Free Guidance (CFG) Ho & Salimans (2022) can be applied *uniformly* across stages. This obviates complex stage-wise guidance schedules Chen et al. (2025); Kynkänniemi et al. (2024) and yields a simpler, robust implementation.

Training with conditional dropout (classifier-free). We train the unified DiT b^θ exactly as in the conditional generation objective shown in equation 19, with the only change that the conditioning signal is randomly dropped. Let \mathbf{c} denote the conditioning signal (e.g., class label or text prompt), and let \emptyset denote the null condition. Define the mixed conditioning

$$\bar{\mathbf{c}} \sim q(\bar{\mathbf{c}}) = (1 - p_\emptyset) p(\mathbf{c}) + p_\emptyset \delta_\emptyset, \tag{66}$$

Algorithm 1 Training a unified multi-stage Flow-Matching model b^θ (ODE view)

Require: Dataset $\mathcal{D} = \{x^{(K)}\} \sim p_{\text{data}}$, stages $k \in \{1, \dots, K\}$ with dimensions d_k , feature-map resolutions r_k and resolution embedding $e_k = E(r_k)$; down/upsamplers $D_k : \mathbb{R}^{d_k} \rightarrow \mathbb{R}^{d_{k-1}}$ and $U_k : \mathbb{R}^{d_{k-1}} \rightarrow \mathbb{R}^{d_k}$, composite downsample $D_{K \rightarrow k}$; time partition $0 = t_0^1 < t_1^1 = t_0^2 < \dots < t_1^K = 1$; noise scales σ (stage 1) and $\{\sigma_k\}_{k=2}^K$; batch size B .

Comment: Ground-truth at stage k is $x_1^{(k)} = D_{K \rightarrow k}(x^{(K)}) \sim \rho_1^{(k)}(\cdot | x^{(K)})$.

1: **for** each training step **do**

2: **for** $i = 1$ to B **do**

3: Sample $x^{(K)} \sim p_{\text{data}}$; sample $t \sim \mathcal{U}[0, 1]$.

4: Find k such that $t \in [t_0^k, t_1^k]$; set the rescaled time $\tau \leftarrow \frac{t - t_0^k}{t_1^k - t_0^k} \in [0, 1]$.

5: **Target at stage k :** $x_1^{(k)} \leftarrow D_{K \rightarrow k}(x^{(K)})$ $\triangleright x_1^{(k)} \sim \rho_1^{(k)}(\cdot | x^{(K)})$

6: **if** $k = 1$ **then** \triangleright Stage 1: noise-to-image coupling is independent

7: Sample $x_0^{(1)} \sim \mathcal{N}(0, \sigma^2 I_{d_1})$ $\triangleright \rho_0^{(1)}(x_0^{(1)})$

8: **else** \triangleright Stage $k > 1$: conditional dependent coupling

9: Sample $\zeta_k \sim \mathcal{N}(0, I_{d_k})$

10: $m_k(x_1^{(k)}) \leftarrow U_k(D_k(x_1^{(k)}))$

11: $x_0^{(k)} \leftarrow m_k(x_1^{(k)}) + \sigma_k \zeta_k$ $\triangleright \rho_0^{(k)}(\cdot | x_1^{(k)}) = \mathcal{N}(m_k, \sigma_k^2 I)$

12: **end if**

13: **Linear interpolant:** $I_\tau^{(k)} \leftarrow (1 - \tau) x_0^{(k)} + \tau x_1^{(k)}$

14: **Target velocity:** $\dot{I}_\tau^{(k)} \leftarrow x_1^{(k)} - x_0^{(k)}$ \triangleright constant in τ for linear path

15: $e_k \leftarrow E(r_k)$ \triangleright resolution embedding

16: $u_\theta \leftarrow b^\theta(I_\tau^{(k)}, \tau, e_k)$ \triangleright DiT vector field shared across stages

17: Per-sample loss: $\ell_i \leftarrow \|u_\theta\|_2^2 - 2 \dot{I}_\tau^{(k)} \cdot u_\theta$ \triangleright equiv. to $\|u_\theta - \dot{I}_\tau^{(k)}\|_2^2$ up to a const.

18: **end for**

19: $\mathcal{L}(\theta) \leftarrow \frac{1}{B} \sum_{i=1}^B \ell_i$ \triangleright matches $\mathbb{E}[\|b^\theta\|^2 - 2 \dot{I} \cdot b^\theta]$

20: Update parameters: $\theta \leftarrow \theta - \eta \nabla_\theta \mathcal{L}(\theta)$

21: **end for**

where $p_\emptyset \in (0, 1)$ is the dropout probability and δ_\emptyset is a point mass at \emptyset . The training loss becomes

$$\mathcal{L}_{\text{cfg}}(\theta) = \mathbb{E}_{\substack{\tau \sim [0, 1], k, e_k, \\ (x_0^{(k)}, x_1^{(k)}) \sim \rho^{(k)}(x_0^{(k)}, x_1^{(k)} | x^{(K)}), \\ \bar{c} \sim q}} \left[\|b^\theta(I_\tau^{(k)}, \tau, e_k, \bar{c})\|^2 - 2 \dot{I}_\tau^{(k)} \cdot b^\theta(I_\tau^{(k)}, \tau, e_k, \bar{c}) \right], \quad (67)$$

with $I_\tau^{(k)} = (1 - \tau)x_0^{(k)} + \tau x_1^{(k)}$, $\dot{I}_\tau^{(k)} = x_1^{(k)} - x_0^{(k)}$, and $\tau = \frac{t - t_0^k}{t_1^k - t_0^k}$ as in Sec. 3.3.

CFG at inference: guided vector field. Let the *conditional* and *unconditional* vector-field predictions be

$$b_{\mathbf{c}}^\theta(z, \tau, e_k) = b^\theta(z, \tau, e_k, \mathbf{c}), \quad b_\emptyset^\theta(z, \tau, e_k) = b^\theta(z, \tau, e_k, \emptyset). \quad (68)$$

Given a global guidance scale $S_{\text{cfg}} \geq 0$ that is *shared across all stages k* , we define the CFG-guided field by the standard linear rule Ho & Salimans (2022):

$$\begin{aligned} b_{\text{cfg}}^\theta(z, \tau, e_k; \mathbf{c}, S_{\text{cfg}}) &= b_\emptyset^\theta(z, \tau, e_k) + S_{\text{cfg}} \left(b_{\mathbf{c}}^\theta(z, \tau, e_k) - b_\emptyset^\theta(z, \tau, e_k) \right) \\ &= (1 - S_{\text{cfg}}) b_\emptyset^\theta + S_{\text{cfg}} b_{\mathbf{c}}^\theta. \end{aligned} \quad (69)$$

This recovers unconditional generation when $S_{\text{cfg}} = 0$, the nominal conditional model when $S_{\text{cfg}} = 1$, and stronger condition-following for $S_{\text{cfg}} > 1$.

Stage-wise conditional generation under coupling. At inference, the state $X_\tau^{(k)}$ in stage k evolves under the guided ODE driven by equation 69:

$$\frac{d}{d\tau} X_\tau^{(k)} = b_{\text{cfg}}^\theta(X_\tau^{(k)}, \tau, e_k; \mathbf{c}, S_{\text{cfg}}), \quad \tau \in [0, 1], \quad (70)$$

Algorithm 2 Inference via sequential multi-stage ODE integration (forward Euler)

Require: Trained vector field b^θ ; stages $k \in \{1, \dots, K\}$ with dimensions d_k , feature-map resolutions r_k and resolution embedding $e_k = E(r_k)$; upsamplers $U_k : \mathbb{R}^{d_{k-1}} \rightarrow \mathbb{R}^{d_k}$; noise scales σ (stage 1) and $\{\sigma_k\}_{k=2}^K$; per-stage step counts $\{N_k\}$.

Comment: The Markovian cascade uses $\hat{x}_0^{(1)} \sim \mathcal{N}(0, \sigma^2 I_{d_1})$ and, for $k \geq 2$, $\hat{x}_0^{(k)} = U_k(\hat{x}_1^{(k-1)}) + \sigma_k \zeta_k$ with $\zeta_k \sim \mathcal{N}(0, I_{d_k})$.

```

1: Initialize stage 1 (noise-to-image): Sample  $\hat{x}_0^{(1)} \sim \mathcal{N}(0, \sigma^2 I_{d_1})$ ; set  $\hat{X}_0^{(1)} \leftarrow \hat{x}_0^{(1)}$ .
2: for  $k = 1$  to  $K$  do
3:    $\Delta\tau \leftarrow 1/N_k$ ;  $e_k \leftarrow E(r_k)$ 
4:   if  $k > 1$  then ▷ Conditional dependent coupling from previous stage
5:     Sample  $\zeta_k \sim \mathcal{N}(0, I_{d_k})$ 
6:      $\hat{x}_0^{(k)} \leftarrow U_k(\hat{x}_1^{(k-1)}) + \sigma_k \zeta_k$ 
7:      $\hat{X}_0^{(k)} \leftarrow \hat{x}_0^{(k)}$ 
8:   end if
9:   for  $n = 0$  to  $N_k - 1$  do
10:     $\tau \leftarrow n \Delta\tau$ 
11:     $\hat{v} \leftarrow b^\theta(\hat{X}_\tau^{(k)}, \tau, e_k)$  ▷ ODE velocity at rescaled time  $\tau \in [0, 1]$ 
12:    Euler step:  $\hat{X}_{\tau+\Delta\tau}^{(k)} \leftarrow \hat{X}_\tau^{(k)} + \Delta\tau \cdot \hat{v}$ 
13:   end for
14:   Stage output:  $\hat{x}_1^{(k)} \leftarrow \hat{X}_1^{(k)}$  ▷ resolution  $d_k$ 
15: end for
16: return  $\hat{x}_1^{(K)} \in \mathbb{R}^{d_K}$  ▷ final high-resolution sample

```

with initial condition

$$X_0^{(1)} = x_0^{(1)} \sim \mathcal{N}(0, \sigma^2 I_{d_1}), \quad X_0^{(k)} = U_k(\hat{x}_1^{(k-1)}) + \sigma_k \zeta_k, \quad \zeta_k \sim \mathcal{N}(0, I_{d_k}), \quad k \geq 2, \quad (71)$$

where the conditional dependent coupling is exactly the construction in equation 9. The stage output is the terminal state

$$\hat{x}_1^{(k)} = X_1^{(k)} = X_0^{(k)} + \int_0^1 b_{\text{cfg}}^\theta(X_t^{(k)}, t, e_k; \mathbf{c}, S_{\text{cfg}}) dt, \quad (72)$$

and the full cascade is obtained by the recursion

$$\hat{x}_1^{(1)} = X_1^{(1)}, \quad \hat{x}_1^{(k)} = X_1^{(k)}(U_k(\hat{x}_1^{(k-1)}) + \sigma_k \zeta_k), \quad k = 2, \dots, K, \quad (73)$$

which is the same Markov structure as equation 16 but with the guided field b_{cfg}^θ .

Remarks. (i) The use of a *single* S_{cfg} across all stages is justified by the fact that, under conditional dependent coupling, each stage already targets the correct $\rho_1^{(k)}(x_1^{(k)} \mid x^{(K)})$. Hence, CFG serves primarily to bias the direction of transport within each accurately learned stage rather than to compensate for a stage mismatch, removing the need for stage-wise tuning. (ii) For an SDE parameterization, the same rule equation 69 is applied to the predicted score/drift in place of b^θ :

$$s_{\text{cfg}}^\theta(z, t, e_k; \mathbf{c}, S_{\text{cfg}}) = s_\varnothing^\theta(z, t, e_k) + S_{\text{cfg}}(s_\mathbf{c}^\theta(z, t, e_k) - s_\varnothing^\theta(z, t, e_k)),$$

and the sampler integrates the corresponding guided stochastic dynamics with $X_0^{(k)}$ as in equation 71. (iii) Following the CFG strategy introduced in this section for conditional generation, we extend the unconditional generation procedure described in Appendix §E, and provide the training and inference procedures of the unified multi-stage generative model b^θ with CFG as shown below.

Algorithm 3 Training a unified multi-stage Flow-Matching model b^θ with Classifier-Free Guidance

Require: Dataset $\mathcal{D} = \{x^{(K)}, \mathbf{c}\}$ with conditions \mathbf{c} (e.g., class/text); stages $k \in \{1, \dots, K\}$ with dimensions d_k , feature-map resolutions r_k and resolution embedding $e_k = E(r_k)$; down/upsamplers $D_k : \mathbb{R}^{d_k} \rightarrow \mathbb{R}^{d_{k-1}}$ and $U_k : \mathbb{R}^{d_{k-1}} \rightarrow \mathbb{R}^{d_k}$; composite downsample $D_{K \rightarrow k}$; time partition $0 = t_0^1 < t_1^1 = t_0^2 < \dots < t_1^K = 1$; noise scales σ (stage 1) and $\{\sigma_k\}_{k=2}^K$; classifier-free dropout probability $p_\emptyset \in (0, 1)$; batch size B .

Comment: Ground-truth at stage k is $x_1^{(k)} = D_{K \rightarrow k}(x^{(K)}) \sim \rho_1^{(k)}(\cdot \mid x^{(K)})$. Conditional dropout samples $\bar{\mathbf{c}}$ from $q(\bar{\mathbf{c}}) = (1 - p_\emptyset)p(\mathbf{c}) + p_\emptyset\delta_\emptyset$.

1: **for** each training step **do**

2: **for** $i = 1$ **to** B **do**

3: Sample $(x^{(K)}, \mathbf{c}) \sim \mathcal{D}$; sample $t \sim \mathcal{U}[0, 1]$.

4: Find k such that $t \in [t_0^k, t_1^k]$; set $\tau \leftarrow \frac{t - t_0^k}{t_1^k - t_0^k} \in [0, 1]$.

5: **Target at stage k :** $x_1^{(k)} \leftarrow D_{K \rightarrow k}(x^{(K)})$.

6: **if** $k = 1$ **then** ▷ Stage 1: noise-to-image, independent prior

7: Sample $x_0^{(1)} \sim \mathcal{N}(0, \sigma^2 I_{d_1})$ ▷ $\rho_0^{(1)}(x_0^{(1)})$

8: **else** ▷ Stage $k > 1$: conditional dependent coupling

9: Sample $\zeta_k \sim \mathcal{N}(0, I_{d_k})$

10: $m_k(x_1^{(k)}) \leftarrow U_k(D_k(x_1^{(k)}))$

11: $x_0^{(k)} \leftarrow m_k(x_1^{(k)}) + \sigma_k \zeta_k$ ▷ $\rho_0^{(k)}(\cdot \mid x_1^{(k)}) = \mathcal{N}(m_k, \sigma_k^2 I)$

12: **end if**

13: **Linear interpolant:** $I_\tau^{(k)} \leftarrow (1 - \tau)x_0^{(k)} + \tau x_1^{(k)}$

14: **Target velocity:** $\dot{I}_\tau^{(k)} \leftarrow x_1^{(k)} - x_0^{(k)}$ ▷ constant in τ for linear path

15: **Conditional dropout:** Draw $u \sim \mathcal{U}[0, 1]$; set $\bar{\mathbf{c}} \leftarrow \emptyset$ if $u < p_\emptyset$, else $\bar{\mathbf{c}} \leftarrow \mathbf{c}$.

16: $e_k \leftarrow E(r_k)$ ▷ resolution embedding fused with time embedding

17: $u_\theta \leftarrow b^\theta(I_\tau^{(k)}, \tau, e_k, \bar{\mathbf{c}})$ ▷ DiT vector field shared across stages

18: Per-sample loss: $\ell_i \leftarrow \|u_\theta\|_2^2 - 2 \dot{I}_\tau^{(k)} \cdot u_\theta$ ▷ matches equation 67

19: **end for**

20: $\mathcal{L}_{\text{cfg}}(\theta) \leftarrow \frac{1}{B} \sum_{i=1}^B \ell_i$

21: Update parameters: $\theta \leftarrow \theta - \eta \nabla_\theta \mathcal{L}_{\text{cfg}}(\theta)$

22: **end for**

Algorithm 4 Inference via sequential multi-stage ODE integration with Classifier-Free Guidance

Require: Trained vector field b^θ ; user condition \mathbf{c} ; global guidance scale $S_{\text{cfg}} \geq 0$ (shared across stages); stages $k \in \{1, \dots, K\}$ with dimensions d_k , feature-map resolutions r_k and resolution embedding $e_k = E(r_k)$; upsamplers $U_k : \mathbb{R}^{d_{k-1}} \rightarrow \mathbb{R}^{d_k}$; noise scales σ (stage 1) and $\{\sigma_k\}_{k=2}^K$; per-stage step counts $\{N_k\}$.
Comment: Guided field $b_{\text{cfg}}^\theta(z, \tau, e_k; \mathbf{c}, S_{\text{cfg}}) = (1 - S_{\text{cfg}})b_\emptyset^\theta(z, \tau, e_k) + S_{\text{cfg}}b_{\mathbf{c}}^\theta(z, \tau, e_k)$, cf. equation 69.

```

1: Initialize stage 1 (noise-to-image): Sample  $\hat{x}_0^{(1)} \sim \mathcal{N}(0, \sigma^2 I_{d_1})$ ; set  $\hat{X}_0^{(1)} \leftarrow \hat{x}_0^{(1)}$ .
2: for  $k = 1$  to  $K$  do
3:    $\Delta\tau \leftarrow 1/N_k$ ;  $e_k \leftarrow E(r_k)$ 
4:   if  $k > 1$  then ▷ Conditional dependent coupling from previous stage
5:     Sample  $\zeta_k \sim \mathcal{N}(0, I_{d_k})$ 
6:      $\hat{x}_0^{(k)} \leftarrow U_k(\hat{x}_1^{(k-1)}) + \sigma_k \zeta_k$ 
7:      $\hat{X}_0^{(k)} \leftarrow \hat{x}_0^{(k)}$ 
8:   end if
9:   for  $n = 0$  to  $N_k - 1$  do
10:     $\tau \leftarrow n \Delta\tau$ 
11:    Unconditional:  $\hat{v}_\emptyset \leftarrow b^\theta(\hat{X}_\tau^{(k)}, \tau, e_k, \emptyset)$ 
12:    Conditional:  $\hat{v}_{\mathbf{c}} \leftarrow b^\theta(\hat{X}_\tau^{(k)}, \tau, e_k, \mathbf{c})$ 
13:    Guided field:  $\hat{v}_{\text{cfg}} \leftarrow (1 - S_{\text{cfg}})\hat{v}_\emptyset + S_{\text{cfg}}\hat{v}_{\mathbf{c}}$  ▷  $S_{\text{cfg}}=0$  uncond.,  $S_{\text{cfg}}=1$  nominal cond.
14:    Euler step:  $\hat{X}_{\tau+\Delta\tau}^{(k)} \leftarrow \hat{X}_\tau^{(k)} + \Delta\tau \cdot \hat{v}_{\text{cfg}}$ 
15:  end for
16:  Stage output:  $\hat{x}_1^{(k)} \leftarrow \hat{X}_1^{(k)}$  ▷ resolution  $d_k$ 
17: end for
18: return  $\hat{x}_1^{(K)} \in \mathbb{R}^{d_K}$  ▷ final high-resolution sample

```

G IMPLEMENT DETAILS

We report the implementation details of our model in Table 3.

Table 3: Complete Parameter Configuration for PixelFlow

Category	Parameter	Value	Description
Model Architecture	num.attention_heads	16	Number of attention heads
	attention.head.dim	72	Dimension of each attention head
	in_channels	3	Input channels (RGB)
	out_channels	3	Output channels (RGB)
	depth	28	Number of transformer layers
	num.classes	1000	Number of ImageNet classes
	patch.size	4	Patch size for patch embedding
	attention.bias	true	Whether to use bias in attention
	embed.dim	1152	Embedding dimension (16×72)
	dropout	0.0	Dropout rate
Scheduler	cross.attention.dim	512	Cross-attention dimension
	max.token.length	512	Maximum token length for text
Scheduler	num.train.timesteps	1000	Number of training timesteps
	num.stages	4	Number of cascade stages
	diminish factor γ	2.0	Flow parameter
Training	lr	1e-4	Learning rate
	weight_decay	0.0	Weight decay
	epochs	10	Number of training epochs
	grad.clip.norm	1.0	Gradient clipping norm
	ema.decay	0.9999	EMA decay rate
Data	logging.steps	10	Logging frequency
	root	/public/datasets/ILSVRC2012/train	Dataset root path
	center.crop	false	Whether to center crop
	resolution	256	Image resolution
	expand_ratio	1.125	Image expansion ratio
	num.workers	4	Number of data loader workers
Data Augmentation	batch.size	4	Batch size per GPU
	RandomHorizontalFlip	true	Random horizontal flip
	RandomCrop	true	Random crop (if not center crop)
	Resize	LANCZOS	Resize interpolation method
	Normalize	[0.5, 0.5, 0.5]	Normalization mean and std
Optimization	optimizer	AdamW	Optimizer type
	Optimizer Hyperparameters	$\beta_1 = 0.9, \beta_2 = 0.95, \epsilon = 1e^{-6}$	Optimizer Hyperparameters
	Learning rate	$1e^{-4}$	Learning rate
	precision	bfloat16	Training precision
	deterministic.ops	false	Deterministic operations
Inference	num.inference.steps	24	Steps per stage (default)
	CFG strength S_{cfg}	3.0	CFG scale (evaluation)
	shift	1.0	Noise shift parameter
	use.ode.dopri5	false	Use ODE solver
	num.fid.samples	50000	Number of FID samples
ODE Solver	sampler.type	dopri5	ODE solver type
	atol	$1e-06$	Absolute tolerance
	rtol	0.001	Relative tolerance
	t0, t1	0, 1	Time range